Scientia Iranica C (2021) 28(3), 1378–1399

SCIENTIA IRANICA

Sharif University of Technology
Scientia Iranica
Transactions C: Chemistry and Chemical Engineering
http://scientiairanica.sharif.edu

A triple-porosity radial composite model for two-phase well test analysis of volatile oil in fractured-vuggy reservoirs

H. Baniasadi[a] and F. Rashidi[b,*]

a. *Department of Petroleum Engineering, Amirkabir University of Technology, Tehran, Iran.*
b. *Department of Chemical Engineering, Amirkabir University of Technology, Tehran, P.O. Box 158754413, Iran.*

Received 25 February 2020; received in revised form 21 November 2020; accepted 4 January 2021

KEYWORDS
Two-phase well-test;
Fractured-vuggy reservoir;
Volatile oil;
Radial composite model;
Triple-porosity.

Abstract. In this study, a novel analytical model of well test analysis was used for characterization of a fractured-vuggy reservoir containing volatile oil with flowing wellbore pressure below the bubble-point pressure. Conducting well test analysis in this medium is challenging due to complications associated with reservoir geology and fluid behavior. Rock-related complications are caused by three media that interact with one another as a result of their different flow behaviors. Fluid-related challenges are caused by gas liberation and two-phase flow near the wellbore. To carry out the analysis, a synthetic model was investigated and the required pressure data were generated that exhibited a radial composite behavior within this reservoir. Then, a triple porosity radial composite model was developed for the analysis and estimation of parameters associated with the mentioned reservoirs. The parameters of the reservoir were predicted using the proposed model with acceptable accuracy. The estimated effective permeabilities in all cases were close to the actual values, with the absolute relative error being less than 0.1. However, the obtained interporosity flow parameters were slightly different from the single-phase parameters due to the presence of gas bank near the wellbore.

1. Introduction

Well testing remains one of the most powerful tools used for characterizing complex reservoirs in recent decades. This progress can be accomplished through development of new interpretation methods as well as use of powerful computers and pressure measurement devices with high accuracy. Well testing is a significant factor in characterization of reservoirs and evaluation of wellbore performance in reservoir management. However, interpretation of well testing in volatile oil and gas condensate reservoirs below the saturation pressure, especially in complex geological structures (e.g., naturally fractured reservoirs), is challenging due to the behavioral complexities of the fluid and reservoir [1,2].

Naturally fractured reservoirs comprise a considerable volume of world oil and gas reserves. Considerable scientific attention has been recently given to the complicated structures of such reserves [3–8]. Carbonate reservoirs are usually composed of fracture and matrix systems, while some others are composed of fracture, matrix, and vug systems. In the past few decades, considerable improvement in the modeling

*. *Corresponding author. Tel.: +98 21 64543190*
E-mail addresses: Baniasadi@aut.ac.ir (H. Baniasadi); Rashidi@aut.ac.ir (F. Rashidi).

doi: 10.24200/sci.2021.55522.4262

and understanding of flow behavior in fractured rock has been made [8–16]. However, a majority of studies have only focused on naturally fractured reservoirs and ignored large cavities. Since a number of fractured-vuggy reservoirs have been found around the world with significant potential of oil and gas reserves, characterization of fractured-vuggy rock has been the focus of some studies [17–22].

Among the generally accepted conceptual models at hand to characterize the fluid flow in fractured reservoirs, the dual-continuum models including double and multi porosity as well as dual-permeability ones are common approaches to modeling fractured reservoirs. In addition to the traditional double-porosity concept, a number of triple-porosity models have been developed to describe the fluid flow through vuggy fractured rocks [19,21–30]. These triple-porosity models have been proposed as extensions to the Warren and Root double-porosity model [10]. Although the proposed triple-porosity models encompass a combination of media including:

(a) Two different types of matrix and fractured network,
(b) Fractured network and continuous matrix and caverns,
(c) Matrix and two fractured networks,
(d) Fractures and vugs and matrix rock,

these analytical solutions can solve the same mathematical model [31]. In fact, these methods focus on modeling the heterogeneity of fractures or rock matrix by subdividing them into two or more subdomains with different properties for single-phase flow in fractured reservoirs [26].

All of the abovementioned analytical models consider only single-phase flow in reservoir. Hence, they are not suitable for some cases where fluid mobility varies in the reservoir such as water/gas injection cases, or for those where two-phase flow occurs near the wellbore such as volatile oil or gas condensate reservoirs. In case the bottom-hole pressure drops below the saturation pressure in volatile oil or gas condensate reservoirs, a two-region radial composite system is generated through two-phase flow near the wellbore and single-phase flow away from it. The existence of the two-phase flow region near the wellbore reduces the oil mobility which makes the pressure derivative curve of a radial homogenous system behave like a "radial composite" one [32,33]. In such cases, an appropriate model is required to characterize the reservoir and obtain its parameters through well test analysis. This study aims to model the volatile oil flow in fractured-vuggy reservoirs.

The objective of the present study was to develop a flow model to characterize fractured vuggy reservoirs containing volatile oil through pressure transient test analysis. To this end, a new analytical model was developed to analyze the volatile oil in fractured vuggy reservoirs. The developed model is a radial composite one that is suitable for all cases behaving as composite systems. To investigate the applicability of the proposed model to well test analysis, a synthetic fractured vuggy reservoir containing volatile oil was built and then, the pressure data versus time for draw-down and build-up tests were generated. Then, the saturation profile around the wellbore as well as the flow behavior during draw-down and build-up tests below the bubble point pressure were investigated. Finally, an in-house program was used for well test analysis by the proposed model. The obtained results indicated that volatile oil in fractured vuggy reservoirs below the bubble point pressure exhibited a radial composite behavior, and the model developed in this study could be used for well test analysis and parameter estimations in such reservoirs with acceptable accuracy. The estimated effective permeabilities in all cases were close to the actual values, with an ARE being less than 0.1. However, the obtained interporosity flow parameters were slightly different from single-phase interporosity flow parameters due to the presence of gas bank around the wellbore.

2. Theory and background

2.1. Fractured-vuggy reservoirs

A typical fractured vuggy reservoir comprises a large number of vugs or cavities of different sizes, large and well-connected fractures, and often low-permeable rock matrix. Vugs are the result of sulfate and/or carbonate dissolution whose sizes vary from millimeters to meters. They are indirectly connected to fractures by small fractures or micro fractures, isolated by rock matrix from fractures, or directly connected to fractures [34]. Figure 1(a) shows an outcrop of a fractured vuggy reservoir layer and Figure 1(b) presents the conceptual model.

In a fractured-vuggy system, similar to the conventional double-porosity concept developed by Warren and Root [10], large fractures are conceptualized as the main path for global flow in the reservoir, while matrix and vuggy continuum, which are locally connected to each other, directly or indirectly interact with the fracture continuum and mainly provide storage spaces as either sink or source. In this system, the directly connected vugs and cavities with fractures are considered as a part of the fracture media, and the isolated vugs within the matrix media are regarded as a part of matrix media (Figure 1(b)).

Since matrix and vugs do not have the same interaction with fracture media and vugs interact with both fracture and matrix continuums, the system

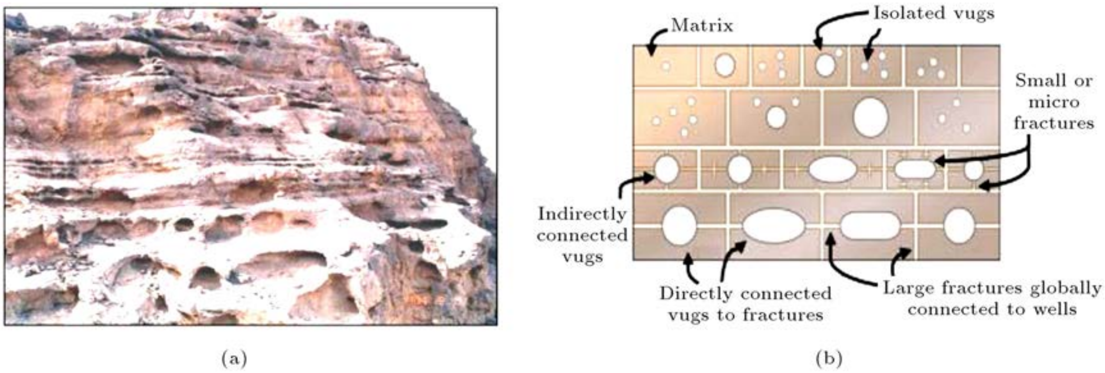

Figure 1. Fractured vuggy formation: (a) An outcrop of a fractured vuggy formation and (b) a conceptual model of fractured vuggy formation [26].

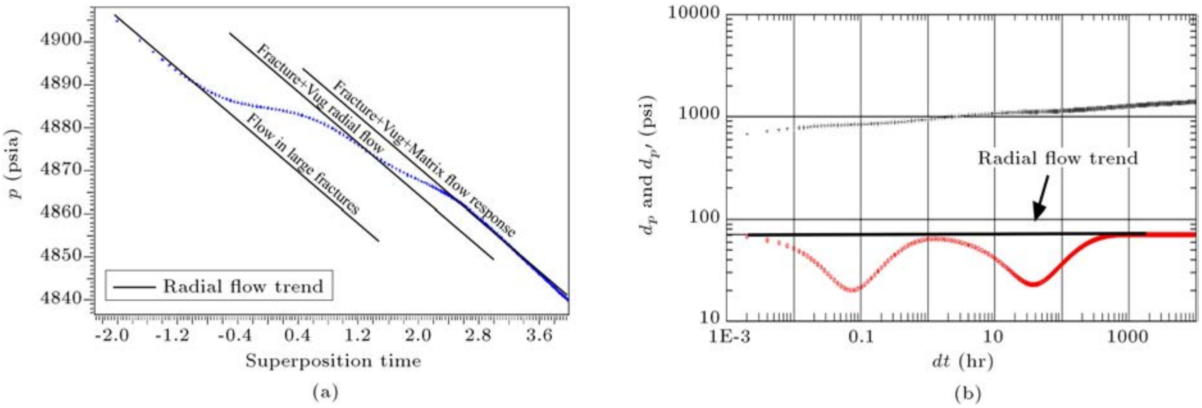

Figure 2. Typical pressure response of flow through a triple-continuum fracture medium: (a) Semi-log plot and (b) log-log plot.

cannot be simplified, assuming that matrix continuum is comprised of matrix and vugs connected to it [21]. However, the fracture-vug-matrix system is conceptualized as a system that includes:

1. "Large" fractures globally connected to wells;
2. Vugs or cavities of different sizes, locally connected to the fracture system by "small" fractures or rock matrix;
3. Rock matrix, locally connected to vugs and/or large fractures (Figure 1(b)).

Almost all flow equations for fractured vuggy reservoirs are developed based on such a conceptual model [26].

Since there are three separate porosities in a fractured vuggy reservoir, the pressure response of the system can show the characteristics of the combined effects. In such systems, the fracture medium, which is globally connected to the wellbore and has the greatest transmissivity, is the first to respond. The cavity and matrix continuum do not flow directly into the wellbore and, thus, respond at later times. The cavity continuum responds faster than the matrix continuum due to its larger transmissivity than that of the matrix. Therefore, in a typical fractured vuggy reservoir with single-phase oil flow through the reservoir, the flow behavior may exhibit three parallel straight lines in a semi-log space (Figure 2(a)). The characteristic behavior is also visible in the log-log pressure derivative presentation in the presence of two interporosity flow "valleys" (Figure 2(b)). In this plot, due to the higher interporosity transmissivity among vugs and fractures, the interporosity flow from the vuggy system through the fracture network into the wellbore is observed first, which can be recognized by the first valley in the derivative plot. To be specific, if the contrast among the interporosity flow parameters is large enough, the second valley in the derivative plot would be observed, corresponding to the fluid transfer from the matrix system to the fracture network [19,27].

2.2. Volatile oil reservoir behavior

In case the flowing wellbore pressure drops below the bubble point pressure during production from volatile oil reservoirs, the multiphase flow occurs near the wellbore due to liberation of dissolved gas in oil [32,35]. Gas liberation around the wellbore reduces oil mobility, thus decreasing the oil effective permeability. Initial gas phase is formed near the wellbore and propagates radially around the well. Gas liberation may create three regions with different fluid mobilities around the wellbore. In regions I and II, close to the wellbore, the pressure is below the bubble point pressure and gas will be liberated from the oil phase. In region I, which is nearest to the well, gas saturation reaches above the critical gas saturation. Hence, both oil and gas are mobile and flow simultaneously toward the well. However, in region II, gas saturation is lower than its critical value and gas is immobile. In region III, away from the well where pressure is above the bubble point pressure of the reservoir fluid, only single-phase oil is present with initial water saturation. regions I and II are referred to as gas banks in the literature. Existence of these three regions and their sizes depends on the reservoir pressure and oil composition. Decrease in oil effective permeability due to gas bank can significantly affect the wellbore performance. The two-phase flow region around the wellbore reduces oil mobility, which makes the pressure derivative curve of a radial homogenous system behave similarly to that of a two-region radial composite system. The first region is an altered one with reduced effective permeability due to two-phase gas and oil flow near the wellbore. The second region away from the wellbore is a virgin zone with original permeability [33,36–43].

Of note, in well test analysis of volatile oil reservoirs with radial composite models, the reservoir is divided into two regions:

(a) The gas bank region near the well bore (referred to as region 1 here);

(b) The single-phase oil zone (referred to as region 2 here).

The radial composite model considers the oil phase and gas phase near the wellbore as the dominant fluid in both regions and fluid heterogeneity, respectively.

3. Mathematical model

As discussed earlier, in volatile oil reservoirs with flowing pressure below the bubble point pressure, the two-phase flow near the wellbore makes a homogenous system behave similarly as a radial composite one. Therefore, a radial composite model is required to study the behavior of volatile oil in fractured vuggy reservoir and to characterize it through the well test data. The present study developed a triple-porosity radial composite model with consideration of pseudo-steady interporosity-flow approximation. This model is an extension of the triple-porosity model originally developed by Liu et al. [19] for fractured vuggy reservoirs. The schematic of the proposed model is presented in Figure 3. It consists of two concentric regions with different rock and fluid properties separated by radial discontinuity. The inner zone radius is R_1 and includes

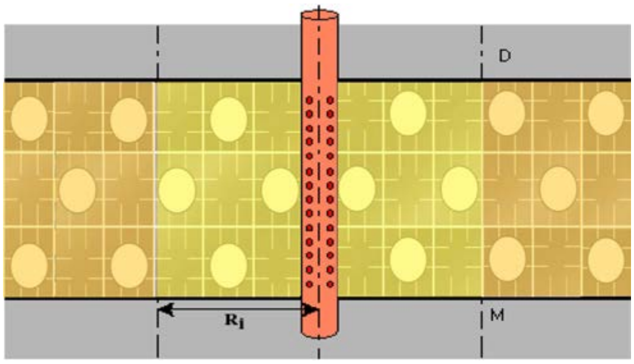

Figure 3. Schematic representation of the triple-porosity radial composite model.

a well of radius r_w located at its center. The outer zone is covered by the single-phase oil and is assumed to be infinite in size. Other assumptions are the same as those presented in the model proposed by Liu et al. [19].

The governing equations describing transient fluid flow in both inner and outer regions of the triple-continuum system are shown in the following:

For the fracture network:

$$\frac{k_{fj}}{\mu_j}\frac{1}{r}\frac{\partial}{\partial r}\left(r\frac{\partial p_{fj}}{\partial r}\right)=\phi_{fj}c_{fj}\frac{\partial p_{fj}}{\partial t}+\phi_{mj}c_{mj}\frac{\partial p_{mj}}{\partial t}+\phi_{vj}c_{vj}\frac{\partial p_{vj}}{\partial t},\qquad j=1,2. \tag{1}$$

For the matrix continuum:

$$\phi_{mj}c_{mj}\frac{\partial p_{mj}}{\partial t}+\alpha_{mf}\frac{k_{mj}}{\mu_j}(p_{mj}-p_{fj})+\alpha_{mv}\frac{k_{mj}}{\mu_j}(p_{mj}-p_{vj})=0,\qquad j=1,2. \tag{2}$$

For the cavity continuum:

$$\phi_{vj}c_{vj}\frac{\partial p_{vj}}{\partial t}+\alpha_{fv}\frac{k_{vj}}{\mu_j}(p_{vj}-p_{fj})-\alpha_{mv}\frac{k_{mj}}{\mu_j}(p_{mj}-p_{vj})=0,\qquad j=1,2. \tag{3}$$

Subscripts f, v, and m are indices of fracture, cavity, and matrix systems, respectively. However, 1 and 2 are indices of the inner and outer regions; p, C, k, and ϕ denote the pressure, total effective compressibility, permeability, and initial porosity of each continuum, respectively. In addition, α_{mf}, α_{mv}, and α_{fv} are the shape factors between different media, depending on the geometry of the interporosity flow and their dimensions are reciprocal of area.

The initial pressure, p_0, is considered as uniform for all three media in the reservoir:

$$p_{fj}(r,0)=p_{mj}(r,0)=p_{mj}(r,0)=p_0, \quad j=1,2. \tag{4}$$

In a radially infinite system, the same constant pressure prevails on the outer boundaries:

$$p_{f2}(\infty,t)=p_{m2}(\infty,t)=p_{v2}(\infty,t)=p_0. \tag{5}$$

A constant volumetric flow rate, q, is assumed to be the inner boundary condition at the wellbore with skin and wellbore storage effects are ignored:

$$\frac{\partial p_{f1}}{\partial r}(r_w,t)=\frac{q\mu}{2\pi r_w k_{f1} h}, \tag{6}$$

where r_w is well radius, μ fluid viscosity, and h the thickness of the flow system.

Dimensionless pressure (P_D), dimensionless time (t_D), and dimensionless radius (r_D) are defined below:

$$p_{Dij}=\frac{2\pi k_{ij}h}{q\mu_j}(p_0-p_{ij}), \tag{7}$$

where i = matrix (m), fracture (f) or vugs (v), and $j=1$ and 2:

$$t_D=\frac{k_{f1}t}{\mu_1 r_w^2(\phi_{m1}c_{m1}+\phi_{f1}c_{f1}+\phi_{v1}c_{v1})}, \tag{8}$$

$$r_D=\frac{r}{r_w}, \tag{9}$$

$$R_D=\frac{R_1}{r_w}. \tag{10}$$

The governing equations (Eqs. (1)–(3)), initial condition (Eq. (4)), and boundary conditions (Eqs. (5) and (6)) take the following forms:

$$\frac{1}{r_D}\frac{\partial}{\partial r_D}\left(r_D\frac{\partial p_{Df1}}{\partial r_D}\right)=\omega_{f1}\frac{\partial p_{Df1}}{\partial t_D}+\omega_{m1}\frac{\partial p_{Dm1}}{\partial t_D}+\omega_{v1}\frac{\partial p_{Dv1}}{\partial t_D}, \tag{11}$$

$$\omega_{m1}\frac{\partial p_{Dm1}}{\partial t_D}+\lambda_{mf1}(p_{Dm1}-p_{Df1})+\lambda_{mv1}(p_{Dm1}-p_{Dv1})=0, \tag{12}$$

$$\omega_{v1}\frac{\partial p_{Dv1}}{\partial t_D}+\lambda_{fv1}(p_{Dv1}-p_{Df1})-\lambda_{mv1}(p_{Dm1}-p_{Dv1})=0, \tag{13}$$

for the inner region, and:

$$\frac{1}{r_D}\frac{\partial}{\partial r_D}\left(r_D\frac{\partial p_{Df2}}{\partial r_D}\right)=\gamma\left(\omega_{f2}\frac{\partial p_{Df2}}{\partial t_D}+\omega_{m2}\frac{\partial p_{Dm2}}{\partial t_D}+\omega_{v2}\frac{\partial p_{Dv2}}{\partial t_D}\right), \tag{14}$$

$$\gamma\omega_{m2}\frac{\partial p_{Dm2}}{\partial t_D}+\lambda_{mf2}(p_{Dm2}-p_{Df2})+\lambda_{mv2}(p_{Dm2}-p_{Dv2})=0, \tag{15}$$

$$\gamma\omega_{v2}\frac{\partial p_{Dv2}}{\partial t_D}+\lambda_{fv2}(p_{Dv2}-p_{Df2})-\lambda_{mv2}(p_{Dm2}-p_{Dv2})=0, \tag{16}$$

for the outer region. Dimensionless initial and boundary conditions become:

Initial condition:

$$p_{Df1,2}(r_D,0)=p_{Dm1,2}(r_D,0)=p_{Dm1,2}(r_D,0)=0. \tag{17}$$

Inner boundary condition:

$$\frac{\partial p_{Df1}}{\partial r_D}(1,t_D)=-1. \tag{18}$$

Interface boundary condition:

$$\frac{\partial p_{Df1}}{\partial r_D}(R_D,t_D)=\frac{1}{M}\frac{\partial p_{Df2}}{\partial r_D}(R_D,t_D), \tag{19}$$

$$p_{Df1}(R_D,t_D)=p_{Df2}(R_D,t_D). \tag{20}$$

Outer boundary condition:

$$p_{Df2}(\infty,t_D)=p_{Dm2}(\infty,t_D)=p_{Dv2}(\infty,t_D)=0. \tag{21}$$

The above system is characterized by three interporosity transmissivity ratios between different systems (i.e., fracture, matrix, and vugs), two storativity ratios (The third interporosity ratio could be defined based on the following correlation: $\omega_m+\omega_v+\omega_f=1.$), a mobility ratio, and a diffusivity ratio between inner and outer zones.

$$\lambda_{mfj}=\alpha_{mf}r_w^2\left(\frac{k_{mj}}{k_{fj}}\right), \qquad j=1,2, \tag{22}$$

$$\lambda_{mvj}=\alpha_{mv}r_w^2\left(\frac{k_{mj}}{k_{fj}}\right), \qquad j=1,2, \tag{23}$$

$$\lambda_{vfj}=\alpha_{vf}r_w^2\left(\frac{k_{vj}}{k_{fj}}\right), \qquad j=1,2, \tag{24}$$

$$\omega_{ij}=\frac{\phi_{ij}c_{ij}}{\phi_{fj}c_{fj}+\phi_{mj}c_{mj}+\phi_{vj}c_{vj}}, \quad i=m,f,v; \quad j=1,2(\omega_{mj}+\omega_{vj}+\omega_{fj}=1), \tag{25}$$

$$M=\left[\frac{k_{f1}/\mu_1}{k_{f2}/\mu_2}\right], \tag{26}$$

$$\gamma=\left[\frac{k_{f1}}{\mu_1(\phi_{f1}c_{f1}+\phi_{m1}c_{m1}+\phi_{v1}c_{v1})}\right]\Big/\left[\frac{k_{f2}}{\mu_2(\phi_{f2}c_{f2}+\phi_{m2}c_{m2}+\phi_{v2}c_{v2})}\right]. \tag{27}$$

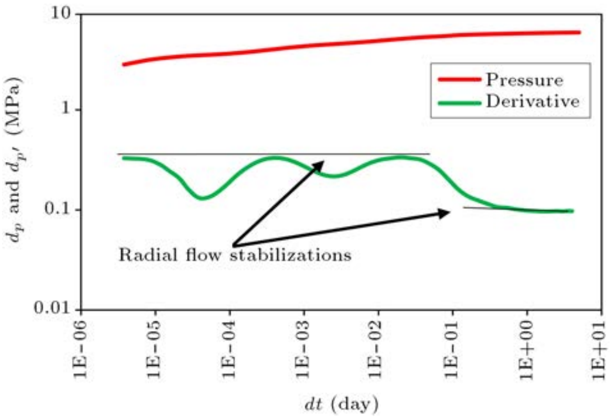

Figure 4. A type curve of triple-porosity radial composite model.

Consequently, the mathematical model is fully defined by Eqs. (11)–(27). These equations are solved for dimensionless pressure, P_{Df1}, at the wellbore with Laplace transformation and inverted numerically using Stehfest [44] algorithm. More details of the solution to the above system of equations are given in the Appendix where the effect of wellbore storage and skin effect are also included by changing the inner boundary condition of the model.

Figure 4 shows a type curve of the developed triple porosity radial composite model. As observed, the model for a fractured vuggy reservoir is characterized by mobility and storativity change in radial direction shown by two radial flow stabilization lines on the log-log pressure derivative curve. The effects of interporosity flow among the fracture, vugs, and matrix are observed on the derivative plot for the inner zone. In fact, the effects caused by interporosity flow on the log-log pressure derivative plots depend on the properties of the rock and fluid. Theoretically, they can be observed on the derivative plot for the inner zone as well as the outer zone or might be totally masked by gas bank effect near the wellbore.

Figure 5 presents the pressure response of a triple-porosity radial composite reservoir with constant distance to the interface at different mobility and storativity ratios. The ratio of the initial to the final derivative level in Figure 5(a) is the ratio of the initial to the final mobility, called M. The effect of storativity ratio on the shape of the derivative curve is presented in Figure 5(b) for $M = 0.5$.

As shown in the following sections, the flow behavior of the volatile oil in a fractured vuggy reservoir is different from that of the single-phase flow in the reservoir and exhibits a radial composite trend similar to the one presented in Figure 4. Analysis of the build-up test data in a fractured vuggy reservoir containing volatile oil facilitates the evaluation of the inner and outer zone effective permeabilities (k_1 and k_2 respectively), wellbore skin (S_w), total skin (S_t), radius of two-phase region near wellbore (R_1), mobility and storativity ratio of different regions (i.e., $(kh/\mu)_{1/2}$ and $(\phi C_t h)_{1/2}$, respectively) [1,32,33,35,45–49]. Moreover, interporosity flow parameters for fracture, vugs, and matrix can be estimated using well test data in case they are not masked by the gas bank effect.

In this study, analytical solutions to the model were obtained in the Laplace space using the Laplace transformation. Stehfest method [44] was then employed to return the solutions to the real-time problem. The nonlinear regression problem for the model amounts to the search of the model parameters that perform the best fits of the pressure and pressure derivative curves. The search for the best-fit parameters is formulated as an optimization problem using genetic algorithm.

4. Reservoir characteristics

Simulation runs were performed to investigate the behavior of fractured vuggy reservoirs containing volatile oil with a flowing wellbore pressure below the bubble

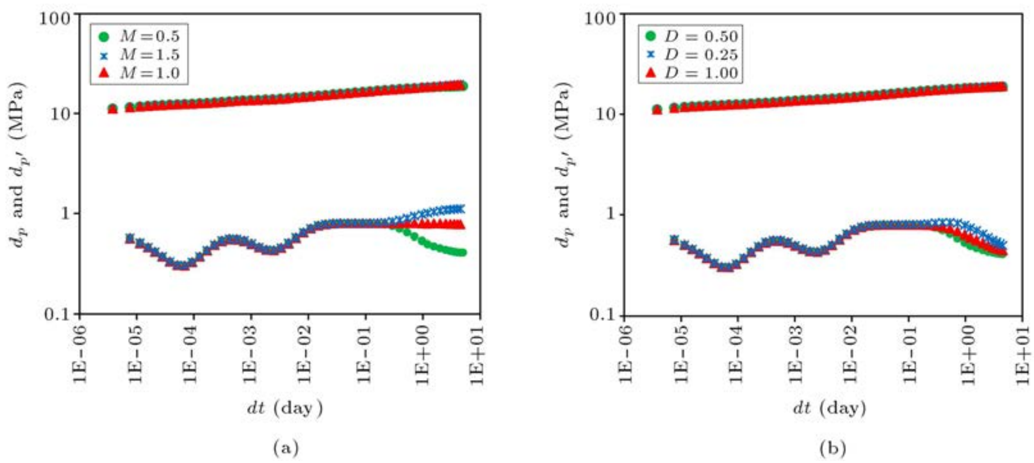

Figure 5. Sensitivity analysis of (a) mobility ratio and (b) storativity ratio.

Table 1. Model parameters (base model).

Parameter	Value	Parameter	Value
Matrix porosity (%)	26	Fracture storativity ratio	0.028
Fracture porosity (%)	1	Vug storativity ratio	0.25
Vug porosity (%)	9	Matrix-fracture transmissivity ratio	5.00E-04
Matrix permeability (m^2)	9.87E-16	Matrix-vug transmissivity ratio	5.00E-08
Fracture permeability (m^2)	4.93E-13	Vug-fracture transmissivity ratio	5.00E-02
Vug permeability (m^2)	9.87E-14	Reservoir temperature (°C)	146
Wellbore radius (m)	0.08	Initial reservoir pressure (MPa)	33.78
Top depth (m)	3048	Wellbore skin	1
Reservoir thickness (m)	30.48		

Table 2. Fluid properties.

Properties	A (base)	B
P_b (MPa)	33.58	28.47
R_s (m^3/m^3)	311.33	505.65
B_o at P_b (m^3/Sm^3)	2.08	2.53

point pressure and to identify the related challenges that might occur in well-test analysis of such reservoirs. To this end, a compositional simulator was used to build the fluid and reservoir models and generate the production data. The reservoir is of single-layered triple-porosity isotropic materials with constant and uniform thickness. The initial temperature and pressure of the reservoir for the base model were 146°C and 33.78 MPa, respectively. Water saturation was assumed to be zero in the matrix, vug, and fracture media. The critical gas and residual oil saturations in the matrix were 5% and 10%, respectively. Table 1 presents the required data for the simulation model.

The radial model was divided into 48 intervals as the primary grid with finer grids around the wellbore and larger ones further away. A triple-porosity mesh was generated from the primary grid including a fracture network with cubic cavity and matrix blocks. This study assumed that there was the pseudo-steady-state interporosity flow among the matrix, fracture and vug systems. To provide smooth saturation profiles and linear pressure gradients, high-resolution time steps, especially at the beginning of each test duration, were taken into account.

Two volatile oil samples, namely A and B, with different volatility characteristics were utilized in this study: sample A, a low volatile oil with a solution gas-oil ratio of 311 m^3/m^3 at the bubble point pressure, and sample B, with highly volatile oil at a solution gas-oil ratio of 506 m^3/m^3 and the bubble point pressure. Fluid properties are presented in Table 2. To model the Pressure-Volume-Temperature (PVT) correlation of the reservoir fluids, Modified Peng-Robinson equation of state with 3 parameters was employed.

Modified Brooks-Corey equations were used to model relative permeability of matrix, as presented by Eqs. (28) and (29) [50]. Three sets of relative permeability curves were employed in this study for the matrix, as presented in Figure 6(a). Table 3 shows the Corey parameters needed for their generation. Linear relative permeability curves for oil and gas were applied to the fracture and vug media in the base case. Since some studies have pointed out that linear relative permeabilities for fracture and vug are not always valid assumptions [51–57], nonlinear relative permeability

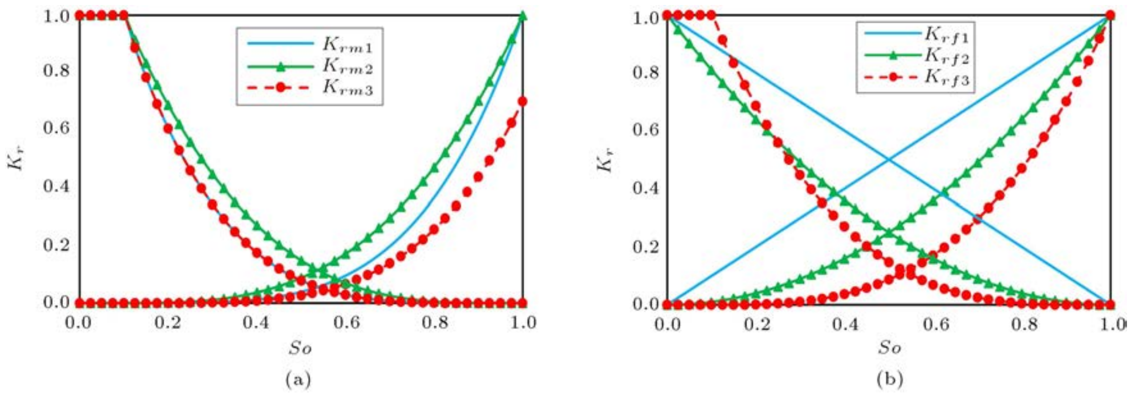

Figure 6. Relative permeability curves: (a) Matrix and (b) fracture.

Table 3. Corey parameters for relative permeability curve generation.

Model	K_{ro}, max	K_{rg}, max	S_{or}	S_{gc}	n_o	n_g
K_{rm1} (base)	1.00	1.00	0.10	0.05	4	4
K_{rm2}	1.00	1.00	0.10	0.05	3	3
K_{rm3}	0.70	1.00	0.10	0.05	4	4
K_{rf1} (linear)	1.00	1.00	0	0	1	1
K_{rf2}	1.00	1.00	0	0	2	2
K_{rf3}	1.00	1.00	0.10	0.05	3	3

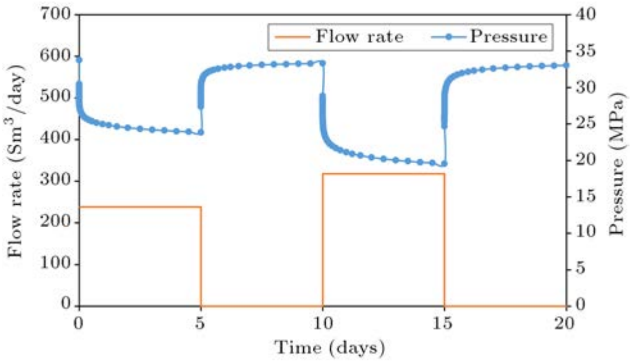

Figure 7. Pressure and rate histories (Case 1).

curves for fracture are also tested.

$$K_{ro} = K_{ro,\max}\left(\frac{S_o - S_{or}}{1 - S_{or} - S_{wc} - S_{gc}}\right)^{n_o}, \qquad (28)$$

$$K_{rg} = K_{rg,\max}\left(\frac{S_g - S_{gc}}{1 - S_{or} - S_{wc} - S_{gc}}\right)^{n_g}. \qquad (29)$$

To investigate the effects of different reservoir conditions, namely the initial reservoir pressure, wellbore skin, fluid type, and relative permeability models, on well test behavior, successive runs including five-day draw-downs and five-day build-ups (DD1, BU1, DD2, and BU2) were performed to generate the synthetic test data. Eight runs were also performed on a variety of cases with different wellbore skins, fluid compositions, and oil-gas relative permeability models. All parameters in simulations were the same as those in the base case, except the ones already reported in the text. Figure 7 shows the pressure and flow rate histories for base case simulation run.

5. Results and discussion

First, the simulation results obtained from synthetic fractured-vuggy reservoir model presented in previous section are discussed. Then, the pressure data generated by the simulation model were examined by the proposed analytical model presented in the mathematical model section.

5.1. Simulation results

In volatile oil reservoirs, when the flowing bottom-hole pressure drops below the bubble point pressure during the draw-down test, a high gas saturation zone with two-phase oil-gas flow is generated near the wellbore. Similar behavior is also observed in multi-porosity systems through all media including the fracture, matrix and vugs. As shown in Figure 8, in draw-down tests, gas saturation increases in the matrix, fracture, and vug systems near the wellbore, and higher production rates would intensify gas liberation. During the subsequent build-up test, the liberated gas around the wellbore may not completely dissolve in the oil due to the fluid composition change occurring near the wellbore during the draw-down test and causing alteration in the saturation pressure in this region. This behavior has been previously discussed in detail for homogenous reservoirs [58]. As shown in Figure 8, in volatile oil reservoirs with wellbore flowing pressure below the bubble point pressure, two-phase oil-gas flow is observed near the wellbore, while only oil flows further away from the wellbore. Two-phase flow near the wellbore in fractured vuggy reservoirs reduces oil mobility, which can be observed in the log-log pressure derivative plots (Figure 9). In a build-up test following a draw-down test with the flowing pressure below the bubble point pressure, a higher level of early time derivative stabilization of the build-up test was observed due to the lower oil relative mobility (see Figure 9(b) for Case 1). This behavior corresponds to the lower mobility at the end of the previous draw-down with the higher level of late time derivative stabilization for the draw-down test, as shown in Figure 9(a). Both of the two-phase draw-down and build-up tests in Figure 9 were compared with a single-phase test with the flowing bottom-hole pressure above the bubble point pressure (Case 2) in which the derivative curve was not affected by the liberated gas near the wellbore. Therefore, the log-log pressure derivative of a fractured vuggy reservoir containing volatile oil below the bubble point pressure is in agreement with the radial composite model with decreasing oil mobility during draw-downs and increasing mobility during the build-ups. This

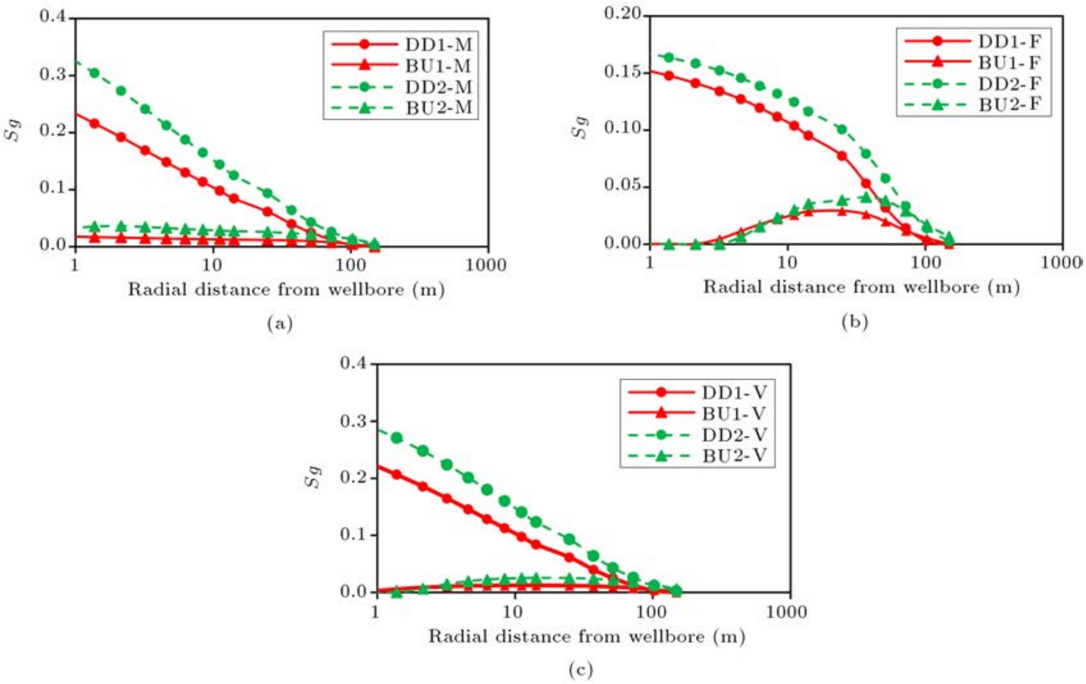

Figure 8. Gas saturation profile at the end of draw-down and build-up tests below P_b in Case 1: (a) Matrix system, (b) fracture system, and (c) vug system.

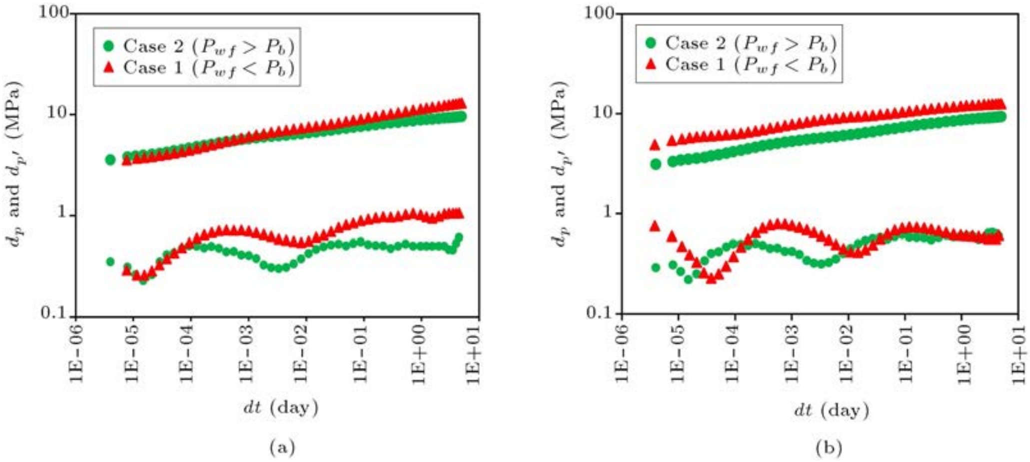

Figure 9. Log-log pressure and derivative of a test in a fractured-vuggy reservoir above and below the bubble point pressure (Cases 1 and 3): (a) Draw-down period and (b) build-up period.

trend is similar to that of the homogeneous volatile oil reservoirs in which the gas bank near wellbore reduces oil mobility and generates a radial composite trend on well test plots due to the gas bank effect [32].

Of note, in black oil reservoirs, the amount of dissolved gas in oil is usually quite low. Hence, in a well test with a bottomhole pressure below the bubble point pressure, there would not be a near wellbore zone with reduced effective permeability. In such cases, the mobility and storativity changes in the radial direction would not be observed in the well test plots, as shown in Figure 10, for a black oil system with American Petroleum Institute (API) gravity of 21. According to this figure, the two-phase well test is similar to the single-phase one in black oil reservoirs. In fact, a black oil reservoir can be regarded as a special case of a volatile oil reservoir with mobility and storativity ratios of one.

The simulation results showed that a change in the relative permeability of the matrix did not affect the pressure derivative curve shape near the wellbore (Figure 11). However, the shape of derivative curve is strongly affected by the relative permeability of fracture. In fact, the saturation profile in the fracture controls the drawdown/buildup derivative curve, as presented in Figures 12 and 13. The oil mobility

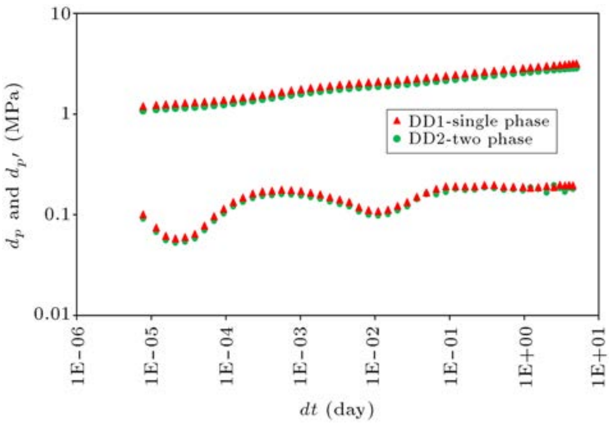

Figure 10. Log-log pressure and derivative of a test in a black oil fractured vuggy reservoir above and below the bubble point pressure.

decreases upon increasing gas saturation inside the fracture media. In the case of linear relative permeability for fractures (K_{rf1}), the amount of the liberated gas inside the fracture near the wellbore is negligible with low changes in the shape of derivative curves. However,

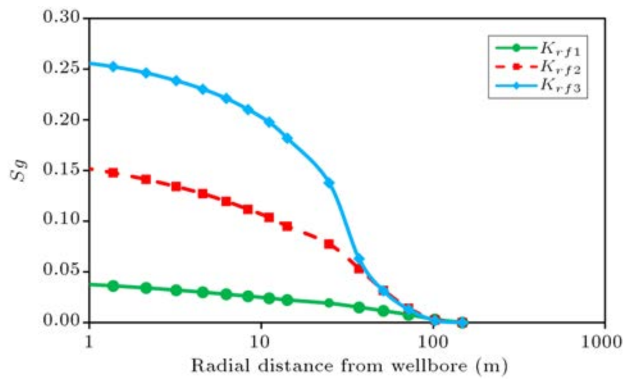

Figure 13. Saturation profiles inside the fracture media near the wellbore in different models.

in cases of non-linear fracture relative permeability (K_{rf2}, K_{rf3}), gas saturation near the wellbore is high that causes significant changes in the derivative curve shape.

To evaluate the effect of initial oil saturation on well test results, sensitivity analysis was performed. In all runs, water phase was assumed to be immobile since

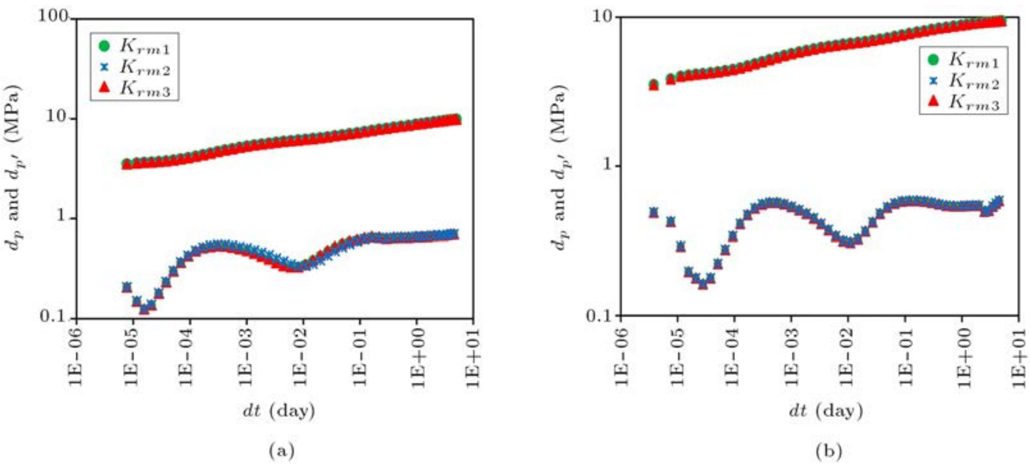

Figure 11. Effect of matrix relative permeability on pressure derivative curves: (a) Drawdown test and (b) build-up test.

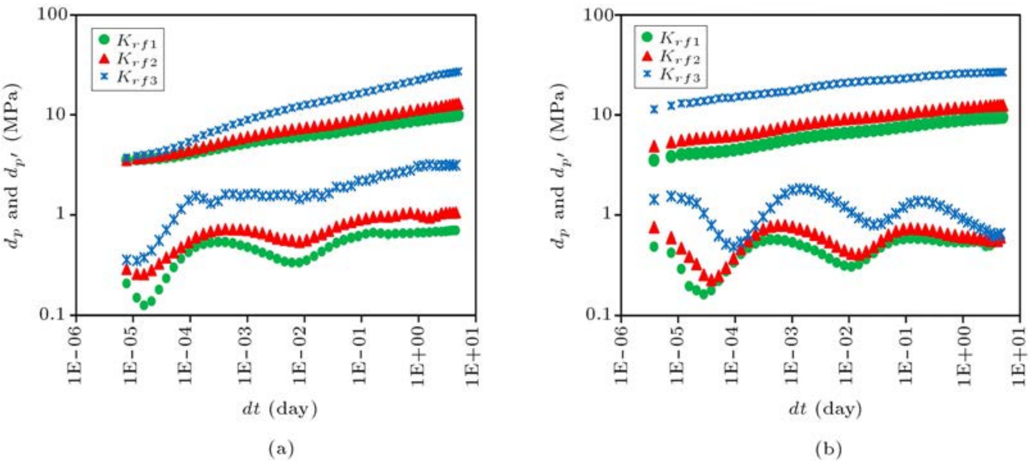

Figure 12. Effect of fracture relative permeability on pressure derivative curves: (a) Drawdown test and (b) build-up test.

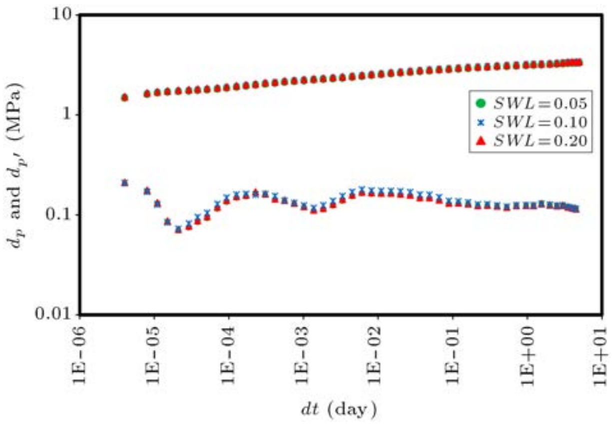

Figure 14. Sensitivity analysis of the effect of immobile water saturation on log-log pressure and derivative curve.

in the proposed model, the effect of water flow on that well test data was ignored. As presented in Figure 14, the presence of immobile water in the reservoir could not affect the well test results.

5.2. Well test analysis

In the previous section, it was revealed that the well test data of the fractured vuggy reservoirs containing volatile oil below the bubble point pressure showed a radial composite trend. In this section, application of the proposed triple-porosity radial composite model was tested to measure the reservoir parameters of the fractured vuggy reservoirs containing volatile oil. An in-house program was generated to compare the simulator output data with those of the proposed model and to determine reservoir parameters using type-curve matching method. Since the draw-down data may be altered by rate fluctuations and wellbore dynamics, the well-test analysis is usually conducted on the build-up test data. The main focus of the following section is on analysis of the build-up tests.

Figure 15 presents the analysis of the first and second build-up tests (BU1 and BU2) in Case 1. The generated model, i.e., triple-porosity radial composite model, produced a good match between the log-log pressure and derivative plots. The log-log derivative curves exhibit two radial-flow stabilizations as an indication of a two-region radial-flow composite behavior. The interporosity flow behavior of the fractured vuggy reservoir is observed in the first stabilization. The second stabilization provides effective reservoir permeability, while the ratio of the first to second stabilization yields mobility ratio $(kh/\mu)_{1/2}$ between the inner zone (two-phase) and outer zone (single-phase). Other parameters such as radius of the two phase region, storativity ratios (ω_f, ω_v), and transmissivity ratio among the matrix, fracture, and vugs (λ_{vf}, λ_{mf}, λ_{vm}) can be subsequently determined by matching the pressure data with the proposed triple-porosity radial composite model.

Table 4 compares the parameters of the simulation model and those evaluated by well test analysis. As observed, there is good agreement between the actual and predicted values of wellbore skin and effective permeability for a single-phase region. Large positive values of total skin are indicative of damage around the wellbore due to gas liberation and oil mobility reduction.

The calculated radius of the gas bank in Table 4 is underestimated compared to the actual radius for both BU1 and BU2 obtained from Figure 8(b). Similar to homogeneous gas condensate systems, the difference between the two results from gas saturation profile variations. The interpreted gas bank radius is smaller than that of the simulator because the gas front is not sharp. Figure 8 shows that gas saturation decreases smoothly along the gas bank. Hence, effective permeability to oil increases gradually. Our radial composite model assumes a sharp permeability change interface.

The calculated interporosity flow parameters presented in Table 4 suggest that when the wellbore pressure drops below the bubble point pressure, in-

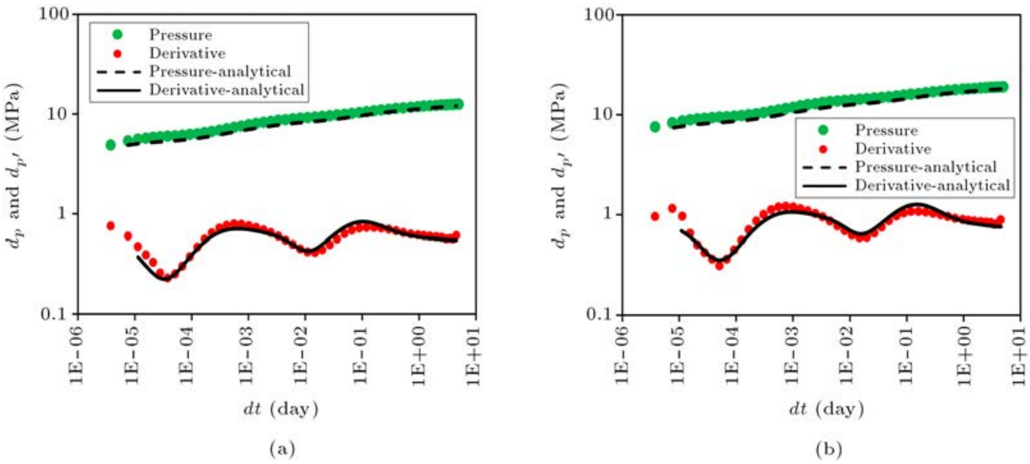

Figure 15. Log-log pressure and derivative plot of (a) BU1 test and (b) BU2 test (Case 1).

Table 4. Results of BU1 and BU2 tests using radial composite model (Case 1).

Parameter	Model value*	BU1		BU2	
		Well test analysis	ARE	Well test analysis	ARE
k_2 (m^2)	4.93E-15	4.82E-15	0.02	4.66E-15	0.06
S_w	1	1.2	0.20	1.25	0.25
S_t		2		3.5	
R_1 (m)		9		8.25	
ω_f	0.028	0.025	0.11	0.025	0.11
ω_v	0.25	0.22	0.12	0.2	0.20
λ_{mf}	5.00E-04	3.70E-04	0.26	4.00E-04	0.20
λ_{mv}	5.00E-08	4.50E-08	0.10	4.30E-08	0.14
λ_{vf}	5.00E-02	3.50E-02	0.30	3.20E-02	0.36

*: Model values are calculated for single-phase flow condition.

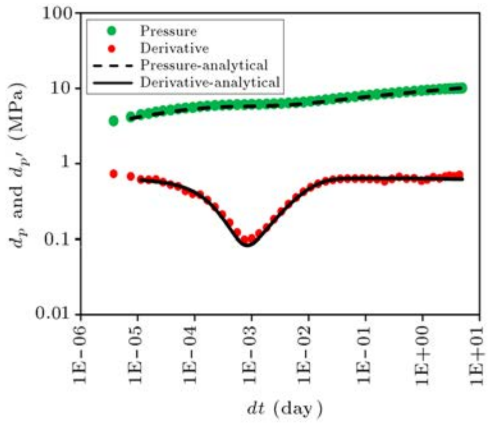

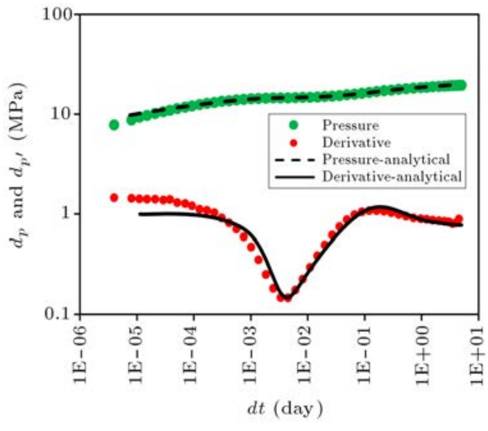

Figure 16. Log-log pressure and derivative plot of test in a dual-porosity system: (a) Above the bubble point pressure and (b) below the bubble point pressure.

terporosity transmissivity ratios decrease with an increase in the gas saturation in fractures with time. Furthermore, the storativity ratios decrease as a result of total compressibility variations in each medium near the wellbore. Any change in the interporosity and storativity parameters of fractured vuggy reservoirs is in agreement with the behavior observed in the fractured gas condensate systems already stated by Al-Baqawi [59].

Then, to examine the accuracy of the proposed model, it was employed to analyze the well test data of a dual-porosity model as a simplified type of triple-porosity systems. To this end, the vug effect was assumed negligible and the system acted as a dual-porosity model. Other parameters were the same as those of the base case (Case 1). To examine the accuracy of the model better, both single-phase and two-phase runs were tested for the model. While in the first drawdown test of this model, the bottomhole pressure was above the bubble point pressure during the entire test, in the second drawdown, the bottomhole pressure fell below the bubble point pressure. The analysis results are presented in Figure 16 and Table 5. As observed earlier, the proposed model for dual-porosity reservoirs could predict the reservoir parameters (permeability, wellbore skin, and interporosity flow parameters) with acceptable accuracy. In the single-phase well test, the predicted parameters were close to the actual ones. In the two-phase run, the interporosity parameters were slightly different since they were affected by two-phase flow near the wellbore.

To evaluate the reliability of the presented method for well test analysis, a variety of triple-porosity systems were analyzed using different model parameters. In Cases 3 and 4, the non-linear relative permeability curves were used in the case of fracture. Case 5 had a higher volatile oil rate than that of the base case; in Case 6, the wellbore skin changed to 5. In all models, other parameters were similar to those of the base case (Case 1). For all scenarios, two stabiliza-

Table 5. Results of BU1 and BU2 tests of dual-porosity model.

Parameter	Model value	BU#1 ($P_{wf} > P_b$)		BU#2 ($P_{wf} < P_b$)	
		Well test analysis	ARE	Well test analysis	ARE
k_2 (m^2)	4.93E-15	5.01E-15	0.01	4.91E-15	0.00
S_w	1	1.2	0.20	1.37	0.37
S_t				3.5	
ω_f	0.037	0.033	0.12	0.030	0.19
ω_v	—	—	—	—	—
λ_{mf}	1.80E-04	1.65E-4	0.08	1.54E-04	0.14
λ_{mv}	—	—	—	—	—
λ_{vf}	—	—	—	—	—

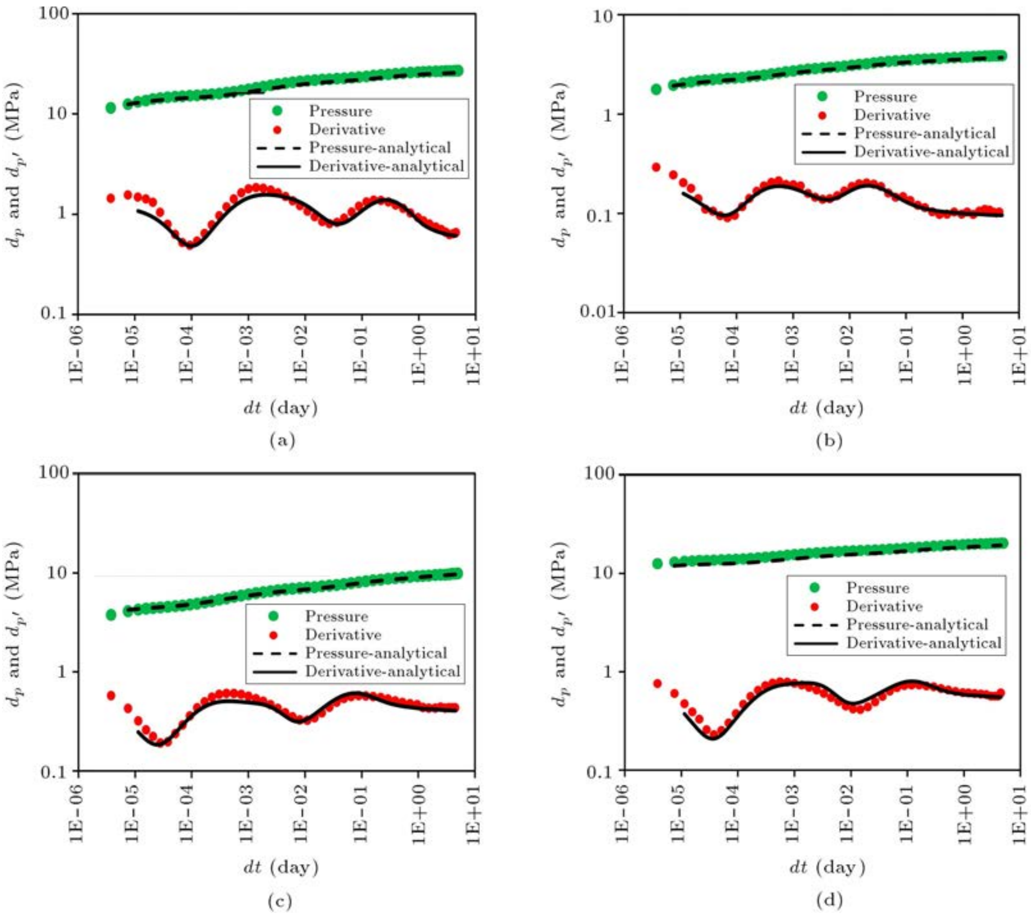

Figure 17. Log-log pressure and derivative of build-up tests in different cases: (a) Case 3: k_{rf2}, (b) Case 4: k_{rf3}, (c) Case 5: Fluid B, and (d) Case 6: $Sw = 5$.

tion levels were visible on the log-log derivative pressure of the build-up test, as shown in Figure 17(a) and (b) for different relative permeability models (Cases 3 and 4), Figure 17(c) for fluid B (Case 5), and Figure 17(d) for non-zero wellbore skin ($Sw = 5$, Case 6). In all cases, a radial composite trend was observed and interporosity flow effects were visible in all derivative plots. Hence, the triple-porosity radial composite model might be used for well test interpretation and parameter estimation. As shown in Figure 17, the selected model yielded consistently similar results in all cases in terms of log-log pressure and derivative, indicating the applicability of the proposed model to well test interpretation.

Table 6 presents the actual model parameters and predicted ones for the aforementioned cases. For

Table 6. Results of BU1 test using radial composite model in different cases.

Parameter	Model value*	Well test result							
		Case 3 (K_{rf2})		Case 4 (K_{rf3})		Case 5 (Fluid B)		Case 6 ($S_w = 5$)	
		Well test analysis	ARE	Well test analysis	ARE	Well test analysis	ARE	Well test analysis	ARE
k_2 (m^2)	4.93E-15	5.23E-15	0.06	4.47E-15	0.09	4.89E-15	0.01	4.70E-15	0.05
S_w	1	1.5	0.50	2.5	1.50	2	1.00	6**	0.20
R_1 (m)		10.5		8.25		7.5		8.5	
ω_f	0.028	0.028	0.01	0.02	0.29	0.027	0.04	0.02	0.29
ω_v	0.25	0.22	0.12	0.17	0.32	0.2	0.20	0.2	0.20
λ_{mf}	5.00E-04	4.30E-04	0.14	3.70E-04	0.26	3.50E-04	0.30	3.80E-04	0.24
λ_{mv}	5.00E-08	4.50E-08	0.10	4.70E-08	0.06	4.40E-08	0.12	4.30E-08	0.14
λ_{vf}	5.00E-02	4.00E-02	0.20	4.30E-02	0.14	3.50E-02	0.30	3.50E-02	0.30

*: Model values are calculated for single-phase flow condition;

**: The wellbore skin value of the model in this case is 5.

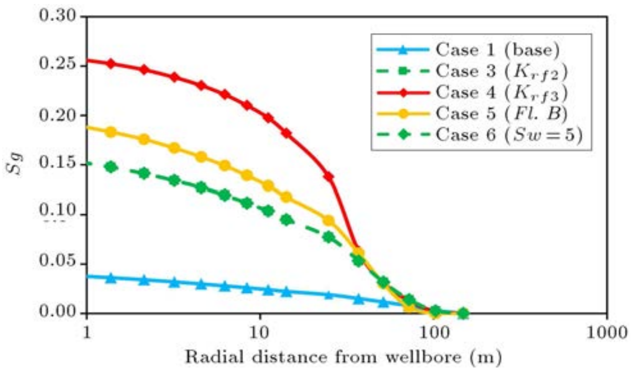

Figure 18. Gas saturation profiles in the fracture at the end of DD1 in different cases.

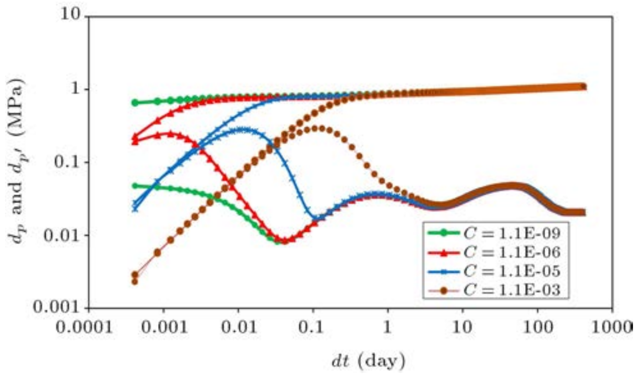

Figure 19. Sensitivity analysis of wellbore storage effect.

all cases, the actual and estimated parameters are in an acceptable range. As expected, the transmissivity ratios (λ_{vf}, λ_{mf}, λ_{vm}) and storativity ratios (ω_f, ω_v) decreased in all cases. Figure 18 presents the gas saturation profile versus distance for different studied cases at the end of draw-downs. A comparison between the actual radius of two-phase regions and predicted ones showed that the radius of the predicted ones was less than that of actual ones, as expected.

In the aforementioned cases, the wellbore storage effect was ignored in the model. In the following, the effect of wellbore storage was investigated. To incorporate the wellbore storage effect in the model, the inner boundary condition for flow equations must be updated, as suggested in the Appendix. Figure 19 shows the well test behavior as well as the effect of wellbore storage on the pressure response, according to which it can be concluded that the wellbore storage can fully mask the presence of the first valley or even both valleys due to the flow from the vuggy continuum. In such cases, the pressure data may be wrongly interpreted as a double-porosity or even a homogeneous reservoir. Therefore, it is strongly recommended that the wellbore storage effect be minimized in the well test operations.

6. Conclusions

The main objective of this study was to investigate the pressure response of volatile oil naturally fractured vuggy reservoir during transient flow periods. The obtained results are listed in the following:

1. A new model was formulated for naturally fractured vuggy reservoirs that exhibited the radial composite behavior and the analytical solution to this model was provided;
2. Volatile oil in fractured vuggy reservoirs below the bubble point pressure showed a radial composite behavior on log-log pressure and derivative plots similar to homogeneous systems;
3. Developed triple-porosity radial composite model could be used for well test analysis and parameter estimation in fractured vuggy reservoirs containing volatile oil with a flowing bottom-hole pressure

below the bubble point pressure. Reservoir parameters (permeability, wellbore skin, and interporosity flow parameters) could be predicted with acceptable accuracy using the proposed model;

4. In the well test analysis of volatile oil in the fractured vuggy reservoirs below the bubble point pressure, the liberated gas could change the interporosity flow behavior in the draw-down and build-up tests. The calculated transmissivity ratios were reduced upon increasing gas saturation near the wellbore and the storativity ratios decreased due to the total compressibility variations of the system near the wellbore.

Nomenclature

ARE	Absolute Relative Error
Bo	Oil formation volume factor (m^3/Sm^3)
BU	Buildup test
C	Wellbore storage
C_D	Dimensionless wellbore storage
C_f	Fracture total compressibility (1/Pa)
C_m	Matrix total compressibility (1/Pa)
C_v	Vug total compressibility (1/Pa)
DD	Drawdown test
dp	Pressure difference (Pa)
dp'	Pressure derivative
h	Formation thickness (m)
$I_0()$	Modified Bessel function of the first kind, zero order
$I_1()$	Modified Bessel function of the first kind, first order
k	Permeability (m^2)
$K_0()$	Modified Bessel function of the second kind, zero order
$K_1()$	Modified Bessel function of the second kind, first order
k_f	Fracture permeability (m^2)
k_m	Matrix permeability (m^2)
k_v	Vug permeability (m^2)
k_{rf}	Fracture relative permeability
k_{rg}	Gas relative permeability
$k_{rg,\max}$	Maximum gas relative permeability
k_{rm}	Matrix relative permeability
k_{ro}	Oil relative permeability
$k_{ro,\max}$	Maximum oil relative permeability
M	Mobility ratio
n_g	Corey exponent for gas relative permeability
n_o	Corey exponent for oil relative permeability
P	Pressure (Pa)
P_b	Bubble point pressure (Pa)
P_i	Initial pressure (Pa)
P_{Df}	Dimensionless fracture pressure
$\overline{p}_{Df}$	Laplace transformed of P_{Df}
P_{Dm}	Dimensionless matrix pressure
$\overline{p}_{Dm}$	Laplace transformed of P_{Dm}
P_{Dv}	Dimensionless vug pressure
$\overline{p}_{Dv}$	Laplace transformed of P_{Dv}
P_{Dw}	Dimensionless wellbore pressure
$\overline{p}_{Dw}$	Laplace transformed of P_{Dw}
P_f	Fracture pressure (Pa)
P_m	Matrix pressure (Pa)
P_r	Reservoir pressure (Pa)
P_v	Vug pressure (Pa)
P_w	Wellbore pressure (Pa)
q	Flow rate (Sm^3/day)
r	Radius (m)
R_1	Two-phase outer radius (m)
r_D	Dimensionless radius
Rs	Solution gas oil ratio (m^3/m^3)
r_w	Wellbore radius (m)
s	Laplace transform
S	Skin
Sg	Gas saturation
Sgc	Critical gas saturation
So	Oil saturation
Sor	Residual oil saturation
St	Total skin
Sw	Wellbore skin
Swc	Critical water saturation
t	Time (days)
t_D	Dimensionless time

Greek letters

λ_{fv}	Fracture-vug transmissivity ratio
λ_{mf}	Matrix-fracture transmissivity ratio
λ_{mv}	Matrix-vug transmissivity ratio
μ	Viscosity (kg/m.s)
ϕ_f	Fracture effective porosity
ϕ_m	Matrix effective porosity
ϕ_v	Vug effective porosity
ω_f	Fracture storativity ratio
ω_m	Matrix storativity ratio

ω_v	Vug storativity ratio
α_{fv}	Fracture-vug interflow shape factor ($1/m^2$)
α_{mf}	Matrix-fracture interflow shape factor ($1/m^2$)
α_{mv}	Matrix-vug interflow shape factor ($1/m^2$)
γ	Diffusivity ratio between two regions

Subscripts and superscripts

b	Bubble point
c	Critical
D	Dimension less
f	Fracture
i	Initial
g	Gas
m	Matrix
o	Oil
r	Relative
t	Total
v	Vug

References

1. Gringarten, A.C., Bozorgzadeh, M., Hashemi, A., and Daungkaew, S. "Well test analysis in lean gas condensate reservoirs: Theory and practice", *SPE Russian Oil and Gas Technical Conference and Exhibition*, Moscow, Russia (2006).
2. Mazloom, J., Kelly, R., and Mahani, H. "A new two-phase pseudo pressure approach for the interpretation of gas condensate well tests in the naturally fractured reservoirs", *SPE Europec/EAGE Annual Conference*, Madrid, Spain (2005).
3. Sarma, P. and Aziz, K. "New transfer functions for simulation of naturally fractured reservoirs with dual porosity models", *SPE Journal*, **11**(3), pp. 328–340 (2006).
4. Bahrami, H., Siavoshi, J., Parvizi, H., et al. "Characterization of fracture dynamic parameters to simulate naturally fractured reservoirs", *International Petroleum Technology Conference*, Kuala Lumpur, Malaysia (2008).
5. Popov, P., Qin, G., Bi, L., et al. "Multiphysics and multiscale methods for modeling fluid flow through naturally fractured carbonate karst reservoirs", *SPE Reservoir Evaluation & Engineering*, **12**(2), pp. 218–231 (2009).
6. Gu, F. and Chalaturnyk, R. "Permeability and porosity models considering anisotropy and discontinuity of coalbeds and application in coupled simulation", *Journal of Petroleum Science and Engineering*, **74**(3), pp. 113–131 (2010).
7. Papi, A., Mohebbi, A., and Eshraghi, S.E. "Numerical simulation of the impact of natural fracture on fluid composition variation through a porous medium", *Journal of Energy Resources Technology*, **141**(4), pp. 042901–042901-16 (2018).
8. Li, M., Li, Q., Bi, G., and Lin, J. "A two-phase flow model for pressure transient analysis of water injection well considering water imbibition in natural fractured reservoirs", *Mathematical Problems in Engineering*, **2018**(1), p. 12 (2018).
9. Barenblatt, G.I., Zheltov, I.P., and Kochina, I.N. "Basic concepts in the theory of seepage of homogeneous liquids in fissured rocks [strata]", *Journal of Applied Mathematics and Mechanics*, **24**(5), pp. 1286–1303 (1960).
10. Warren, J. and Root, P.J. "The behavior of naturally fractured reservoirs", *Society of Petroleum Engineers Journal*, **3**(3), pp. 245–255 (1963).
11. Pruess, K. "A practical method for modeling fluid and heat flow in fractured porous media", *Society of Petroleum Engineers Journal*, **25**(1), pp. 14–26 (1985).
12. Kazemi, H. "Pressure transient analysis of naturally fractured reservoirs with uniform fracture distribution", *Society of Petroleum Engineers Journal*, **9**(4), pp. 451–462 (1969).
13. Wang, S., Cheng, L., Xue, Y., et al. "A semi-analytical method for modeling two-phase flow behavior in fractured carbonate oil reservoirs", *Journal of Energy Resources Technology*, **141**(7), pp. 072902–072902-11 (2019).
14. Al-Bemani, A.S. and Ershaghi, I. "Two-phase flow interporosity effects on pressure transient test response in naturally fractured reservoirs", *Annual Technical Conference and Exhibition of the Society of Petroleum Engineers*, Dallas, USA (1991).
15. Aguilera, R. and Ng, M.G. "Well test analysis of naturally fractured gas condensate reservoirs", *JCPT*, **38**, pp. 55–60 (1999).
16. Gerami, S., Pooladi-Darvish, M., and Mattar, L. "Decline curve analysis for naturally fractured gas reservoirs: A study on the applicability of "pseudo-time" and "material balance pseudo-time"", *International Petroleum Technology Conference* (2007).
17. Kossack, C. and Gurpinar, O. "A methodology for simulation of vuggy and fractured reservoirs", *SPE Reservoir Simulation Symposium* (2001).
18. Rivas-Gomez, S., Gonzalez-Guevara, J.A., Cruz-Hernandez, J., et al. "Numerical simulation of oil displacement by water in a vuggy fractured porous medium", *SPE Reservoir Simulation Symposium* (2001).
19. Liu, J., Bodvarsson, G.S., and Wu, Y.-S. "Analysis of flow behavior in fractured lithophysal reservoirs", *Journal of Contaminant Hydrology*, **62–63**, pp. 189–211 (2003).

20. Hidajat, I., Mohanty, K.K., Flaum, M., and Hirasaki, G. "Study of vuggy carbonates using NMR and X-Ray CT scanning", *SPE Reservoir Evaluation & Engineering*, **7**(5), pp. 365–377 (2004).

21. Camacho Velazquez, R., Vasquez-Cruz, M.A., Castrejon-Aivar, R., and Arana-Ortiz, V. "Pressure transient and decline curve behaviors in naturally fractured vuggy carbonate reservoirs", *SPE Reservoir Evaluation & Engineering*, **8**(2), pp. 95–111 (2005).

22. Kang, Z., Wu, Y., Li, J., et al. "Modeling multiphase flow in naturally fractured vuggy petroleum reservoirs", *SPE Annual Technical Conference and Exhibition,* San Antonio, Texas, USA (2006).

23. Wu, Y. and Ge, J. "The transient flow in naturally fractured reservoirs with three-porosity systems", *Acta, Mechanica Sinica, Theoretical and Applied Mechanics, Beijing, China*, **15**(1), pp. 81–85 (1983).

24. Abdassah, D. and Ershaghi, I. "Triple-porosity systems for representing naturally fractured reservoirs", *SPE Formation Evaluation*, **1**(2), pp. 113–127 (1986).

25. Bai, M., Elsworth, D., and Roegiers, J.C. "Multiporosity/multipermeability approach to the simulation of naturally fractured reservoirs", *Water Resources Research*, **29**(6), pp. 1621–1633 (1993).

26. Wu, Y.-S., Di,. Y., Kang, Z., and Fakcharoenphol, P. "A multiple-continuum model for simulating singlephase and multiphase flow in naturally fractured vuggy reservoirs", *Journal of Petroleum Science and Engineering*, **78**(1), pp. 13–22 (2011).

27. Wu, Y.-S., Ehlig-Economides, C.A., Qin, G., et al. "A triple-continuum pressure-transient model for a naturally fractured vuggy reservoir", *SPE Annual Technical Conference and Exhibition*, California, USA (2007).

28. Wu, Y.-S., Qin, G., Ewing, R., et al. "A multiplecontinuum approach for modeling multiphase flow in naturally fractured vuggy petroleum reservoirs", *International Oil & Gas Conference and Exhibition*, China (2006).

29. Wu, Y.-S., Liu, H.H., and Bodvarsson, G.S. "A triplecontinuum approach for modeling flow and transport processes in fractured rock", *Journal of Contaminant Hydrology*, **73**(1–4), pp. 145–179 (2004).

30. Nie, R., Meng, Y., Yang, Z., et al. "New flow model for the triple media carbonate reservoir", *International Journal of Computational Fluid Dynamics*, **25**(2), pp. 95–104 (2011).

31. Arana, V.H., Pena Chaparro, O., and Cortes, E. "a practical numerical approach for modeling multiporosity naturally fractured reservoirs", *SPE Latin American and Caribbean Petroleum Engineering Conference*, Cartagena, Colombia (2009).

32. Sanni, M.O. and Gringarten, A.C. "Well test analysis in volatile oil reservoirs", *SPE Annual Technical Conference and Exhibition*, Denver, Co, USA (2008).

33. Gringarten, A.C., Al-Lamki, A., Daungkaew, S., et al. "Well test analysis in gas-condensate reservoirs", *SPE Annual Technical Conference and Exhibition*, Dallas, Texas (2000).

34. Gómez, S., Ramos, G., Mesejo, A., et al. "Well test analysis of naturally fractured vuggy reservoirs with an analytical triple porosity-double permeability model and a global optimization method", *Oil & Gas Science and Technology-Revue d'IFP Energies Nouvelles*, **69**(4), pp. 653–671 (2014).

35. Sharifi, M. and Ahmadi, M. "Two-phase flow in volatile oil reservoir using two-phase pseudo-pressure well test method", *Journal of Canadian Petroleum Technology*, **48**(9), pp. 6–11 (2009).

36. Jones, J. and Raghavan, R. "Interpretation of flowing well response in gas-condensate wells (includes associated papers 19014 and 19216)", *SPE Formation Evaluation*, **3**(3), pp. 578–594 (1988).

37. Raghavan, R. "Well-test analysis for multiphase flow", *SPE Formation Evaluation*, **4**(4), pp. 585–594 (1989).

38. Daungkaew, S., Ross, F., and Gringarten. A. "Well test investigation of condensate drop-out behaviour in a North Sea lean gas condensate reservoir", *Paper SPE 77548, presented at the SPE Annual Technical Conference and Exhibition*, San Antonio, TX, September (2002).

39. Barrios, K., Stewart, G., and Davies, D. "A novel methodology for the analysis of well test responses in gas condensate reservoirs", *SPE Latin American and Caribbean Petroleum Engineering Conference*, Port-of-Spain, Trinidad and Tobago (2003).

40. Mazloom, J. and Rashidi, F. "Use of two-phase pseudo pressure method to calculate condensate bank size and well deliverability in gas condensate reservoirs", *Petroleum Science and Technology*, **24**(2), pp. 145–156 (2006).

41. Al Ghamdi, B.N., Ayala, H., and Luis, F. "Evaluation of transport properties effect on the performance of gas-condensate reservoirs using compositional simulation", *Journal of Energy Resources Technology*, **139**(3), pp. 032910–032910-10 (2017).

42. Mohammadi-Khanaposhtani, M., Bahramian, A., and Pourafshary, P. "Disjoining pressure and gas condensate coupling in gas condensate reservoirs", *Journal of Energy Resources Technology*, **136**(4), pp. 042911–042911-6 (2014).

43. Yi, Y., Li, J., and Ji, L. "Numerical determination of critical condensate saturation in gas condensate reservoirs", *Journal of Energy Resources Technology*, **139**(6), pp. 062801–062801-11 (2017).

44. Stehfest, H. "Numerical inversion of Laplace transforms algorithm", *ACM*, **13**(1), pp. 47–49 (1970).

45. Brown, L. "Pressure transient behavior of the composite reservoir", *SPE Annual Technical Conference and Exhibition*, Las Vegas, Nevada (1985).

46. OlarewaJu, J.S., Lee, J.W., and Lancaster, D.E. "Type-and decline-curve analysis with composite models", *SPE Formation Evaluation*, **6**(1), pp. 79–85 (1991).
47. Bozorgzadeh, M. and Gringarten, A.C. "New estimate for the radius of a condensate bank from well test data using dry gas pseudo-pressure", *Society of Petroleum Engineers*, Houston, Texas, USA (2004).
48. Bozorgzadeh, M. and Gringarten, A.C. "Application of build-up transient pressure analysis to well deliverability forecasting in gas condensate reservoirs using single-phase and two-phase pseudo-pressures", *SPE Europec/EAGE Annual Conference*, Madrid, Spain (2005).
49. Bozorgzadeh, M. and Gringarten, A.C. "Condensate bank characterization from well test data and fluid PVT properties", *SPE Reservoir Evaluation & Engineering*, **9**(5), pp. 596–611 (2006).
50. Goda, H.M. and Behrenbruch, P. "Using a modified brooks-corey model to study oil-water relative permeability for diverse pore structures", *SPE Asia Pacific Oil and Gas Conference and Exhibition*, Perth, Australia (2004).
51. Lian, P. and Cheng, L. "The characteristics of relative permeability curves in naturally fractured carbonate reservoirs", *Journal of Canadian Petroleum Technology*, **51**(2), pp. 137–142 (2012).
52. Noroozi, M., Moradi, B., and Bashiri, G. "Effects of fracture properties on numerical simulation of a naturally fractured reservoir", *Trinidad and Tobago Energy Resources Conference*, Port of Spain, Trinidad, p. 12 (2010).
53. Deghmoum, A.H., Tiab, D., and Mazouzi, A. "Relative permeability in dual porosity porous media", *Journal of Canadian Petroleum Technology*, **40**(12), p. 11 (2001).
54. Rossen, W.R. and Kumar, A.T.A. "Effect of fracture relative permeabilities on performance of naturally fractured reservoirs", *International Petroleum Conference and Exhibition of Mexico*, Veracruz, Mexico, p. 12 (1994).
55. Pieters, D.A. and Graves, R.M. "Fracture relative permeability: Linear or non-linear function of saturation", *International Petroleum Conference and Exhibition of Mexico*, Veracruz, Mexico, p. 10 (1994).
56. Aguilera, R. "Relative permeability concepts for predicting the performance of naturally fractured reservoirs", *Journal of Canadian Petroleum Technology*, **21**(5), p. 9 (1982).
57. Chen, C.-Y., Li, K., and Horne, R.N. "Experimental study of phase transformation effects on relative permeabilities in fractures", *SPE Reservoir Evaluation & Engineering*, **10**(5), p. 13 (2007).
58. Baniasadi, H. and Rashidi, F. "Volatile oil well test analysis: application of two-phase pseudo-pressure approach", *Journal of Petroleum Exploration and Production Technology*, **2019**, pp. 1–10 (2019).
59. AlBaqawi, A.M. and Al-Malki, B.H. "Well test analysis in naturally fractured gas condensate reservoirs below dew point pressure", *SPE Asia Pacific Oil and Gas Conference and Exhibition*, Jakarta, Indonesia (2009).

Appendix

Here, the partial differential equations describing the fluid flow in a triple-porosity radial composite system are presented. According to Figure 3, the model consists of two concentric regions with different rock and fluid properties separated by radial discontinuity. The inner zone includes a well of radius r_w located at its center and the radius of this zone is R_1. The outer zone was assumed to be infinite in size. Other assumptions are the same as those in the model proposed by the model of Liu et al. [19]. The partial differential equations for fluid flow in this reservoir system are given below.

For the near wellbore region (region 1):

$$\frac{k_{f1}}{\mu_1}\frac{1}{r}\frac{\partial}{\partial r}\left(r\frac{\partial p_{f1}}{\partial r}\right)=\phi_{f1}c_{f1}\frac{\partial p_{f1}}{\partial t}+\phi_{m1}c_{m1}\frac{\partial p_{m1}}{\partial t}+\phi_{v1}c_{v1}\frac{\partial p_{v1}}{\partial t}, \tag{A.1}$$

$$\phi_{m1}c_{m1}\frac{\partial p_{m1}}{\partial t}+\alpha_{mf}\frac{k_{m1}}{\mu_1}(p_{m1}-p_{f1})+\alpha_{mv}\frac{k_{m1}}{\mu_1}(p_{m1}-p_{v1})=0, \tag{A.2}$$

$$\phi_{v1}c_{v1}\frac{\partial p_{v1}}{\partial t}+\alpha_{fv}\frac{k_{v1}}{\mu_1}(p_{v1}-p_{f1})-\alpha_{mv}\frac{k_{m1}}{\mu_1}(p_{m1}-p_{v1})=0. \tag{A.3}$$

For the outer region (region 2):

$$\frac{k_{f2}}{\mu_2}\frac{1}{r}\frac{\partial}{\partial r}\left(r\frac{\partial p_{f2}}{\partial r}\right)=\phi_{f2}c_{f2}\frac{\partial p_{f2}}{\partial t}+\phi_{m2}c_{m2}\frac{\partial p_{m2}}{\partial t}+\phi_{v2}c_{v2}\frac{\partial p_{v2}}{\partial t}, \tag{A.4}$$

$$\phi_{m2}c_{m2}\frac{\partial p_{m2}}{\partial t}+\alpha_{mf}\frac{k_{m2}}{\mu_2}(p_{m2}-p_{f2})+\alpha_{mv}\frac{k_{m2}}{\mu_2}(p_{m2}-p_{v2})=0, \tag{A.5}$$

$$\phi_{v2}c_{v2}\frac{\partial p_{v2}}{\partial t}+\alpha_{fv}\frac{k_{v2}}{\mu_2}(p_{v2}-p_{f2})-\alpha_{mv}\frac{k_{m2}}{\mu_2}(p_{m2}-p_{v2})=0. \tag{A.6}$$

The initial and boundary conditions of the system are as follows.

Initial condition:

$$p_{f1,2}(r,0) = p_{m1,2}(r,0) = p_{v1,2}(r,0) = p_0. \tag{A.7}$$

Inner boundary condition:

$$\frac{\partial p_{f1}}{\partial r}(r_w,t) = \frac{q\mu}{2\pi r_w k_{f1} h}. \tag{A.8}$$

To incorporate the wellbore storage and skin in the analytical model, the inner boundary must be updated. The inner boundary condition at the wellbore with a constant flow rate q subject to wellbore storage effects and skin region around the wellbore is given below:

$$p_w = \left[p_{f1} - S r_w \frac{\partial p_{f1}}{\partial r}\right]_{r=r_w}, \tag{A.9}$$

$$-C\frac{\partial p_w}{\partial t} + \frac{2\pi r_w k_{f1} h}{\mu}\frac{\partial p_{f1}}{\partial t}(r_w,t) = q. \tag{A.10}$$

Interface boundary condition:

$$\frac{k_{f1}}{\mu_1}\frac{\partial p_{f1}}{\partial r}(R_1,t) = \frac{k_{f2}}{\mu_2}\frac{\partial p_{f2}}{\partial r}(R_1,t), \tag{A.11}$$

$$p_{f1}(R_1,t) = p_{f2}(R_1,t). \tag{A.12}$$

Outer boundary condition:

$$p_{f2}(\infty,t) = p_{m2}(\infty,t) = p_{v2}(\infty,t) = p_0. \tag{A.13}$$

Eqs. (A.1)–(A.6) can be written in a dimensionless form, as shown in the following:

$$\frac{1}{r_D}\frac{\partial}{\partial r_D}\left(r_D\frac{\partial p_{Df1}}{\partial r_D}\right) = \omega_{f1}\frac{\partial p_{Df1}}{\partial t_D} + \omega_{m1}\frac{\partial p_{Dm1}}{\partial t_D} + \omega_{v1}\frac{\partial p_{Dv1}}{\partial t_D}, \tag{A.14}$$

$$\omega_{m1}\frac{\partial p_{Dm1}}{\partial t_D} + \lambda_{mf1}(p_{Dm1} - p_{Df1}) + \lambda_{mv1}(p_{Dm1} - p_{Dv1}) = 0, \tag{A.15}$$

$$\omega_{v1}\frac{\partial p_{Dv1}}{\partial t_D} + \lambda_{fv1}(p_{Dv1} - p_{Df1}) - \lambda_{mv1}(p_{Dm1} - p_{Dv1}) = 0, \tag{A.16}$$

$$\frac{1}{r_D}\frac{\partial}{\partial r_D}\left(r_D\frac{\partial p_{Df2}}{\partial r_D}\right) = \gamma\left(\omega_{f2}\frac{\partial p_{Df2}}{\partial t_D} + \omega_{m2}\frac{\partial p_{Dm2}}{\partial t_D} + \omega_{v2}\frac{\partial p_{Dv2}}{\partial t_D}\right), \tag{A.17}$$

$$\gamma\omega_{m2}\frac{\partial p_{Dm2}}{\partial t_D} + \lambda_{mf2}(p_{Dm2} - p_{Df2}) + \lambda_{mv2}(p_{Dm2} - p_{Dv2}) = 0, \tag{A.18}$$

$$\gamma\omega_{v2}\frac{\partial p_{Dv2}}{\partial t_D} + \lambda_{fv2}(p_{Dv2} - p_{Df2}) - \lambda_{mv2}(p_{Dm2} - p_{Dv2}) = 0. \tag{A.19}$$

The initial and boundary conditions in a dimensionless form are:

Initial condition:

$$p_{Df1,2}(r_D,0) = p_{Dm1,2}(r_D,0) = p_{Dv1,2}(r_D,0) = 0. \tag{A.20}$$

Inner boundary condition:

$$p_{Dw} = \left[p_{Df1} - S\frac{\partial p_{Df1}}{\partial r_D}\right]_{r_D=1}, \tag{A.21}$$

$$C_D\frac{\partial p_{Dw}}{\partial t_D} - \left(\frac{\partial p_{Df1}}{\partial r_D}\right)_{r_D=1} = 1, \tag{A.22}$$

Interface boundary condition:

$$\frac{\partial p_{Df1}}{\partial r_D}(R_D,t_D) = \frac{1}{M}\frac{\partial p_{Df2}}{\partial r_D}(R_D,t_D), \tag{A.23}$$

$$p_{Df1}(R_D,t_D) = p_{Df2}(R_D,t_D). \tag{A.24}$$

Outer boundary condition:

$$p_{Df2}(\infty,t_D) = p_{Dm2}(\infty,t_D) = p_{Dv2}(\infty,t_D) = 0. \tag{A.25}$$

The dimensionless parameters used in the equations above are defined as follows:

$$p_{Dij} = \frac{2\pi k_{ij} h}{q\mu_j}(p_0 - p_{ij}), \quad i = m,f,v; \quad j = 1,2, \tag{A.26}$$

$$p_{Dw} = \frac{2\pi k_{f1} h}{q\mu_1}(p_0 - p_w), \tag{A.27}$$

$$t_D = \frac{k_{f1} t}{\mu_1 r_w^2(\phi_{m1}c_{m1} + \phi_{f1}c_{f1} + \phi_{v1}c_{v1})}, \tag{A.28}$$

$$r_D = \frac{r}{r_w}, \tag{A.29}$$

$$R_D = \frac{R_1}{r_w}, \tag{A.30}$$

$$C_D = \frac{0.8936C}{\phi c_t h r_w^2}, \tag{A.31}$$

$$\omega_{ij} = \frac{\phi_{ij}c_{ij}}{\phi_{fj}c_{fj} + \phi_{mj}c_{mj} + \phi_{vj}c_{vj}}, \quad i = m,f,v; \quad j = 1,2, \tag{A.32}$$

$$\lambda_{mfj} = \alpha_{mf} r_w^2\left(\frac{k_{mj}}{k_{fj}}\right), \qquad j = 1,2, \tag{A.33}$$

$$\lambda_{mvj} = \alpha_{mv} r_w^2\left(\frac{k_{mj}}{k_{fj}}\right), \qquad j = 1,2, \tag{A.34}$$

$$\lambda_{vfj} = \alpha_{vf} r_w^2 \left(\frac{k_{vj}}{k_{fj}}\right), \qquad j = 1,2, \tag{A.35}$$

$$M = \left[\frac{k_{f1}/\mu_1}{k_{f2}/\mu_2}\right], \tag{A.36}$$

$$\gamma = \left[\frac{k_{f1}}{\mu_1(\phi_{f1}c_{f1} + \phi_{m1}c_{m1} + \phi_{v1}c_{v1})}\right] \Big/ \left[\frac{k_{f2}}{\mu_2(\phi_{f2}c_{f2} + \phi_{m2}c_{m2} + \phi_{v2}c_{v2})}\right]. \tag{A.37}$$

Applying Laplace transformation to Eqs. (A.14)–(A.19) yields:

$$\frac{1}{r_D}\frac{\partial}{\partial r_D}\left(r_D\frac{\partial \overline{p}_{Df1}}{\partial r_D}\right) = \omega_{f1} s\overline{p}_{Df1} + \omega_{m1} s\overline{p}_{Dm1} + \omega_{v1} s\overline{p}_{Dv1}, \tag{A.38}$$

$$\omega_{m1} s\overline{p}_{Dm1} + \lambda_{mf1}\left(\overline{p}_{Dm1} - \overline{p}_{Df1}\right) + \lambda_{mv1}\left(\overline{p}_{Dm1} - \overline{p}_{Dv1}\right) = 0, \tag{A.39}$$

$$\omega_{v1} s\overline{p}_{Dv1} + \lambda_{fv1}\left(\overline{p}_{Dv1} - \overline{p}_{Df1}\right) - \lambda_{mv1}\left(\overline{p}_{Dm1} - \overline{p}_{Dv1}\right) = 0, \tag{A.40}$$

$$\frac{1}{r_D}\frac{\partial}{\partial r_D}\left(r_D\frac{\partial \overline{p}_{Df2}}{\partial r_D}\right) = \gamma\left(\omega_{f2} s\overline{p}_{Df2} + \omega_{m2} s\overline{p}_{Dm2} + \omega_{v2} s\overline{p}_{Dv2}\right), \tag{A.41}$$

$$\gamma\omega_{m2} s\overline{p}_{Dm2} + \lambda_{mf2}\left(\overline{p}_{Dm2} - \overline{p}_{Df2}\right) + \lambda_{mv2}\left(\overline{p}_{Dm2} - \overline{p}_{Dv2}\right) = 0, \tag{A.42}$$

$$\gamma\omega_{v2} s\overline{p}_{Dv2} + \lambda_{fv2}\left(\overline{p}_{Dv2} - \overline{p}_{Df2}\right) - \lambda_{mv2}\left(\overline{p}_{Dvm2} - \overline{p}_{Df2}\right) = 0. \tag{A.43}$$

The initial and boundary conditions (Eqs. (A.20)–(A.25)) in Laplace space are as follows:

Initial condition:

$$\overline{p}_{Dm1,2} = \overline{p}_{Df1,2} = \overline{p}_{Dv1,2} = 0. \tag{A.44}$$

Inner boundary condition:

$$\overline{p}_{Dw} = \left[\overline{p}_{Df1} - S\frac{\partial \overline{p}_{Df1}}{\partial r_D}\right]_{r_D=1}, \tag{A.45}$$

$$C_D s\frac{\partial \overline{p}_{Dw}}{\partial t_D} - \left(\frac{\partial \overline{p}_{Df1}}{\partial r_D}\right)_{r_D=1} = \frac{1}{s}, \tag{A.46}$$

$$\frac{\partial \overline{p}_{Df1}}{\partial r_D}(1,s) = \frac{-1}{s}. \tag{A.47}$$

Interface boundary condition:

$$\frac{\partial \overline{p}_{Df1}}{\partial r_D}(R_D,s) = \frac{1}{M}\frac{\partial \overline{p}_{Df2}}{\partial r_D}(R_D,s), \tag{A.48}$$

$$\overline{p}_{Df1}(R_D,s) = \overline{p}_{Df2}(R_D,s). \tag{A.49}$$

Outer boundary condition:

$$\overline{p}_{Df2}(\infty,s) = \overline{p}_{Dm2}(\infty,s) = \overline{p}_{Dv2}(\infty,s) = 0, \tag{A.50}$$

where $\overline{p}_{Dij}$ ($i = m,f,v$; $j = 1,2$) are transformed functions of p_{Dij} in the Laplace domain and s is the transformation variable.

Eqs. (A.39) and (A.40) can be written in the following form:

$$(\omega_{m1}s+\lambda_{mf1}+\lambda_{mv1})\overline{p}_{Dm1} - \lambda_{mv1}\overline{p}_{Dv1} = \lambda_{mf1}\overline{p}_{Df1}, \tag{A.51}$$

$$-\lambda_{mv1}\overline{p}_{Dm1} + (\omega_{v1}s+\lambda_{fv1}+\lambda_{mv1})\overline{p}_{Dv1} = \lambda_{fv1}\overline{p}_{Df1}. \tag{A.52}$$

The solutions to Eqs. (A.51) and (A.52) based on Cramer's rule are given below:

$$\overline{p}_{Dm1} = \frac{\lambda_{mf1}(\omega_{v1}s + \lambda_{fv1} + \lambda_{mv1}) + \lambda_{mv1}\lambda_{fv1}}{(\omega_{m1}s+\lambda_{mf1}+\lambda_{mv1})(\omega_{v1}s+\lambda_{fv1}+\lambda_{mv1}) - \lambda_{mv1}^2} \times \overline{p}_{Df1} = A_1\overline{p}_{Df1}, \tag{A.53}$$

$$\overline{p}_{Dv1} = \frac{\lambda_{fv1}(\omega_{m1}s + \lambda_{mf1} + \lambda_{mv1}) + \lambda_{mf1}\lambda_{mv1}}{(\omega_{m1}s+\lambda_{mf1}+\lambda_{mv1})(\omega_{v1}s+\lambda_{fv1}+\lambda_{mv1}) - \lambda_{mv1}^2} \times \overline{p}_{Df1} = B_1\overline{p}_{Df1}. \tag{A.54}$$

Substituting the values above into Eq. (A.38) yields:

$$\frac{1}{r_D}\frac{\partial}{\partial r_D}\left(r_D\frac{\partial \overline{p}_{Df1}}{\partial r_D}\right) = \omega_{f1} s\overline{p}_{Df1} + \omega_{m1} sA_1\overline{p}_{Df1} + \omega_{v1} sB_1\overline{p}_{Df1} = sf_1(s)\overline{p}_{Df1}, \tag{A.55}$$

where $f_1(s)$ is defined as:

$$f_1(s) = \omega_{f1} + \omega_{m1}A_1 + \omega_{v1}B_1. \tag{A.56}$$

Similarly, Eqs. (A.42) and (A.43) can be written in the following form:

$$(\gamma\omega_{m2}s+\lambda_{mf2}+\lambda_{mv2})\overline{p}_{Dm2} - \lambda_{mv2}\overline{p}_{Dv2} = \lambda_{mf2}\overline{p}_{Df2}, \tag{A.57}$$

$$-\lambda_{mv2}\overline{p}_{Dm2} + (\gamma\omega_{v2}s+\lambda_{fv2}+\lambda_{mv2})\overline{p}_{Dv2} = \lambda_{fv2}\overline{P}_{Df2}. \tag{A.58}$$

The solutions to Eqs. (A.57) and (A.58) are given below:

$$\overline{p}_{Dm2} = \frac{\lambda_{mf2}(\gamma\omega_{v2}s+\lambda_{fv2}+\lambda_{mv2})+\lambda_{mv2}\lambda_{fv2}}{(\gamma\omega_{m2}s+\lambda_{mf2}+\lambda_{mv2})(\gamma\omega_{v2}s+\lambda_{fv2}+\lambda_{mv2})-\lambda_{mv2}^2} \times \overline{p}_{Df2} = A_2\overline{p}_{Df2}, \tag{A.59}$$

$$\overline{p}_{Dv2} = \frac{\lambda_{fv2}(\gamma\omega_{m2}s+\lambda_{mf2}+\lambda_{mv2})+\lambda_{mf2}\lambda_{mv2}}{(\gamma\omega_{m2}s+\lambda_{mf2}+\lambda_{mv2})(\gamma\omega_{v2}s+\lambda_{fv2}+\lambda_{mv2})-\lambda_{mv2}^2} \times \overline{p}_{Df2} = B_2\overline{p}_{Df2}. \tag{A.60}$$

Substituting the above values into Eq. (A.41) gives:

$$\frac{1}{r_D}\frac{\partial}{\partial r_D}\left(r_D\frac{\partial\overline{p}_{Df2}}{\partial r_D}\right) = \gamma\left(\omega_{f2}s\overline{p}_{Df2} + \omega_{m2}sA_2\overline{p}_{Df2} + \omega_{v2}sB_2\overline{p}_{Df2}\right) = sf_2(s)\overline{p}_{Df2}, \tag{A.61}$$

where $f_2(s)$ is defined as:

$$f_2(s) = \gamma(\omega_{f2} + \omega_{m2}A_2 + \omega_{v2}B_2). \tag{A.62}$$

The solutions to the modified Bessel Eqs. (A.55) and (A.61) are:

$$\overline{p}_{Df1} = C_1I_0\left(r_D\sqrt{sf_1(s)}\right) + C_2K_0\left(r_D\sqrt{sf_1(s)}\right), \tag{A.63}$$

$$\overline{p}_{Df2} = C_3I_0\left(r_D\sqrt{sf_2(s)}\right) + C_4K_0\left(r_D\sqrt{sf_2(s)}\right), \tag{A.64}$$

where C_1, C_2, C_3, and C_4 are constants to be defined by boundary conditions.

Inner boundary condition:

$$\overline{P}_{Dw} = C_1I_0\left(\sqrt{sf_1(s)}\right) + C_2K_0\left(\sqrt{sf_1(s)}\right) - S\left[C_1\sqrt{sf_1(s)}I_1\left(\sqrt{sf_1(s)}\right) - C_2\sqrt{sf_1(s)}K_1\left(\sqrt{sf_1(s)}\right)\right], \tag{A.65}$$

$$C_Ds\left[C_1I_0\left(\sqrt{sf_1(s)}\right) + C_2K_0\left(\sqrt{sf_1(s)}\right) - S\left[C_1\sqrt{sf_1(s)}I_1\left(\sqrt{sf_1(s)}\right) - C_2\sqrt{sf_1(s)}K_1\left(\sqrt{sf_1(s)}\right)\right]\right] - \left[C_1\sqrt{sf_1(s)}I_1\left(\sqrt{sf_1(s)}\right) - C_2\sqrt{sf_1(s)}K_1\left(\sqrt{sf_1(s)}\right)\right] = \frac{1}{s}. \tag{A.66}$$

Outer boundary condition:

$$C_3I_0\left(r_D\sqrt{sf_2(s)}\right) + C_4K_0\left(r_D\sqrt{sf_2(s)}\right) = 0 \rightarrow C_3 = 0. \tag{A.67}$$

Interface boundary condition:

$$C_1\sqrt{sf_1(s)}I_1\left(R_D\sqrt{sf_1(s)}\right) - C_2\sqrt{sf_1(s)}K_1\left(R_D\sqrt{sf_1(s)}\right) + \frac{C_4\sqrt{sf_2(s)}}{M}K_1\left(R_D\sqrt{sf_2(s)}\right) = 0, \tag{A.68}$$

$$C_1I_0\left(R_D\sqrt{sf_1(s)}\right) + C_2K_0\left(R_D\sqrt{sf_1(s)}\right) - C_4K_0\left(R_D\sqrt{sf_2(s)}\right) = 0. \tag{A.69}$$

Eqs. (A.66)–(A.69) are simultaneously solved for four unknowns C_1, C_2, C_3, and C_4 based on Cramer's rule:

$$a_{11}C_1 + a_{12}C_2 = -1/s, \tag{A.70}$$

$$a_{21}C_1 + a_{22}C_2 + a_{23}C_4 = 0, \tag{A.71}$$

$$a_{31}C_1 + a_{32}C_2 + a_{33}C_4 = 0. \tag{A.72}$$

with:

$$a_{11} = C_Ds\left[I_0\left(\sqrt{sf_1(s)}\right) - S\sqrt{sf_1(s)}I_1\left(\sqrt{sf_1(s)}\right)\right] - \sqrt{sf_1(s)}I_1\left(\sqrt{sf_1(s)}\right), \tag{A.73}$$

$$a_{12} = C_Ds\left[K_0\left(\sqrt{sf_1(s)}\right) + S\sqrt{sf_1(s)}K_1\left(\sqrt{sf_1(s)}\right)\right] + \sqrt{sf_1(s)}K_1\left(\sqrt{sf_1(s)}\right), \tag{A.74}$$

$$a_{21} = \sqrt{sf_1(s)}I_1\left(R_D\sqrt{sf_1(s)}\right), \tag{A.75}$$

$$a_{22} = -\sqrt{sf_1(s)}K_1\left(R_D\sqrt{sf_1(s)}\right), \tag{A.76}$$

$$a_{23} = \frac{\sqrt{sf_2(s)}}{M}K_1\left(R_D\sqrt{sf_2(s)}\right), \tag{A.77}$$

$$a_{31} = I_0\left(R_D\sqrt{sf_1(s)}\right), \tag{A.78}$$

$$a_{32} = K_0\left(R_D\sqrt{sf_1(s)}\right), \tag{A.79}$$

$$a_{34} = -K_0\left(R_D\sqrt{sf_2(s)}\right). \tag{A.80}$$

C_1 and C_2 are obtained by solving the equations above:

$$C_1 = \frac{\frac{-1}{s}\left(a_{22}a_{23} - a_{23}a_{32}\right)}{a_{11}(a_{22}a_{33} - a_{23}a_{32}) - a_{12}\left(a_{21}a_{33} - a_{23}a_{31}\right)}, \tag{A.81}$$

$$C_2 = \frac{-a_{21}\left(\frac{-1}{s}a_{33}\right) + a_{31}\left(\frac{-1}{s}a_{23}\right)}{a_{11}(a_{22}a_{33} - a_{23}a_{32}) - a_{12}\left(a_{21}a_{33} - a_{23}a_{31}\right)}. \tag{A.82}$$

The solution to the dimensionless bottom hole pressure (P_{Dw}) in real space can be easily obtained using the Stehfest numerical inversion for $\overline{p}_{Dw}$ back to P_{Dw}.

Biographies

Hamid Baniasadi is a PhD candidate in Petroleum Engineering at Amirkabir University of Technology (AUT). He has 6 years of experience in the field of petroleum engineering, having worked in the Oil, Gas, and Petrochemical Research Center of AUT. He holds a BSc degree in Petroleum Engineering and MSc degree in Reservoir Engineering from Amirkabir University of Technology (AUT).

Fariborz Rashidi is a Professor of Chemical Engineering at Amirkabir University of Technology (AUT). His research interests include combustion (simulation and mathematical modeling of combustion, air pollution), thermodynamics (thermodynamics of wax and asphaltene), heat transfer (force convection, porous media, renewable energy), petroleum engineering, environment, HSE, and fluid transport (fluid flow in porous media). He holds a PhD degree in Chemical Engineering (combustion and safety) from the Imperial College of Science and Technology (London, England), an MSc degree in Chemical Engineering (process analysis and development) from the University of Aston (Birmingham, England), and a BSc in Chemical Engineering from Shiraz University (Shiraz, Iran).